ELSEVIER

Contents lists available at ScienceDirect

# Precambrian Research

journal homepage: www.elsevier.com/locate/precamres





# Precise U-Pb age models refine Neoproterozoic western Laurentian rift initiation, correlation, and Earth system changes

Carol Dehler<sup>a,\*</sup>, Mark Schmitz<sup>b</sup>, Abigail Bullard<sup>a,c</sup>, Susannah Porter<sup>d</sup>, Mike Timmons<sup>e</sup>, Karl Karlstrom<sup>f</sup>, Hannah Cothren<sup>a</sup>

- a Utah State University, Logan, UT 84322-4505, USA
- <sup>b</sup> Boise State University, Boise, ID 83725-1535, USA
- <sup>c</sup> Provost & Pritchard Consulting Group, Fresno, CA 93711, USA
- <sup>d</sup> University of California, Santa Barbara, Santa Barbara, CA 93106, USA
- e New Mexico Bureau of Geology and Mineral Resources, New Mexico Tech, Socorro, NM 87801, USA
- f University of New Mexico, Albuquerque, NM 87131, USA

#### ARTICLE INFO

#### Keywords: Chuar Group Pahrump Group Uinta Mountain Group Tonian Bayesian

#### ABSTRACT

The upper Tonian ChUMP (Chuar-Uinta Mountains-Pahrump) strata of the southwestern U.S.A. are hypothesized to be regional correlatives and to record a time of rift basin evolution commencing at ca. 770 Ma in western Laurentia (modern-day coordinates). We test this correlation using U-Pb chemical abrasion-isotope dilution-thermal ionization mass spectrometry (CA-ID-TIMS) on detrital zircon grains from basal units within these successions. ChUMP units yield CA-ID-TIMS maximum depositional ages (MDA) between 775 and 766 Ma: the Chuar Group of AZ has an MDA of 770.1  $\pm$  0.5 Ma (n = 1) and an additional young zircon mode at 775.7  $\pm$  0.3 Ma (n = 11); the Uinta Mountain Group of northern UT has an MDA of 766.3  $\pm$  0.5 Ma (n = 5) and contains a second young mode at 775.1  $\pm$  0.7 Ma (n = 3); and the basal Horse Thief Springs Formation of the middle Pahrump Group CA has an MDA of 775.4  $\pm$  0.7 Ma (n = 3). The ca. 775 and 770 Ma grains are interpreted to be from zircon-bearing mafic sources related to the 770–778 Ma Gunbarrel Large Igneous Province of Yukon and NW U.S.A. The 766 Ma population was either derived from the Mt Rogers complex of eastern Laurentia or could have come from conjugate margins that were in the process of rifting away, such as Tasmania.

The CA-ID-TIMS dates on the Chuar Group in Grand Canyon anchor a Bayesian age model for evaluating late Tonian Earth systems. Faster sediment accumulation rates (80+150/-44 m/My) in the lower Chuar Group are consistent with the inception of an extensional basin related to Rodinia breakup; slower rates in the upper Chuar Group (25+12/-5 m/My) record are associated with relatively deeper water sedimentation and concomitant organic carbon burial during marine transgression. The model also constrains the timing of several biological events recorded in the Chuar Group, including eukaryovorous predation (>767 Ma), the first appearance of vase-shaped microfossils (~741 Ma), and the ranges of *Cerebrosphaera globosa* (=C. buickii; 800–743 Ma) and *Lanulatisphaera laufeldii*.

(766–740 Ma), both proposed as possible marine index fossils for late Tonian time. Finally, the model can also be used to search for stratigraphic evidence of a purported glaciation at ca. 751 Ma.

# 1. Introduction

U-Pb detrital zircon geochronology is revolutionary in constraining the maximum depositional ages of siliciclastic sedimentary successions that otherwise lack dateable material or time-specific index fossils, particularly those of Precambrian age. New high-precision geochronology from the Chuar, the Uinta Mountain, and the middle Pahrump

("ChUMP") groups of SW Laurentia provides an example of a highresolution approach to calibrate depositional ages from ancient strata, and constrain initiation of basin formation and the incipient rifting of western Laurentia from the supercontinent Rodinia. Also dated during previous U-Pb and Re-Os geochronologic studies, these are some of the best dated, fossiliferous late Tonian sedimentary successions in the world (Figs. 1, 2; Porter and Knoll, 2000; Karlstrom et al., 2000; Dehler

E-mail address: carol.dehler@usu.edu (C. Dehler).

<sup>\*</sup> Corresponding author.

et al., 2010; Mahon et al., 2014a, Mahon et al., 2014b; Dehler et al., 2017; Rooney et al 2018). The large body of geochronological data already in existence reflects the importance of these units as reference sections for studies of Neoproterozoic Earth systems. These rocks document, 1)intracratonic basin formation related to continental

extension of Rodinia (Timmons et al., 2001; Li et al., 2008; Dehler et al. 2010; Li et al., 2013; Mahon et al., 2014a, Mahon et al., 2014b); 2) abundant microfossils exhibiting diversity and complexity of life rarely chronicled in Neoproterozoic rocks (Ford and Breed, 1973; Licari, 1978; Bloeser, 1985; Horodyski, 1993; Porter and Knoll, 2000; Porter et al.,

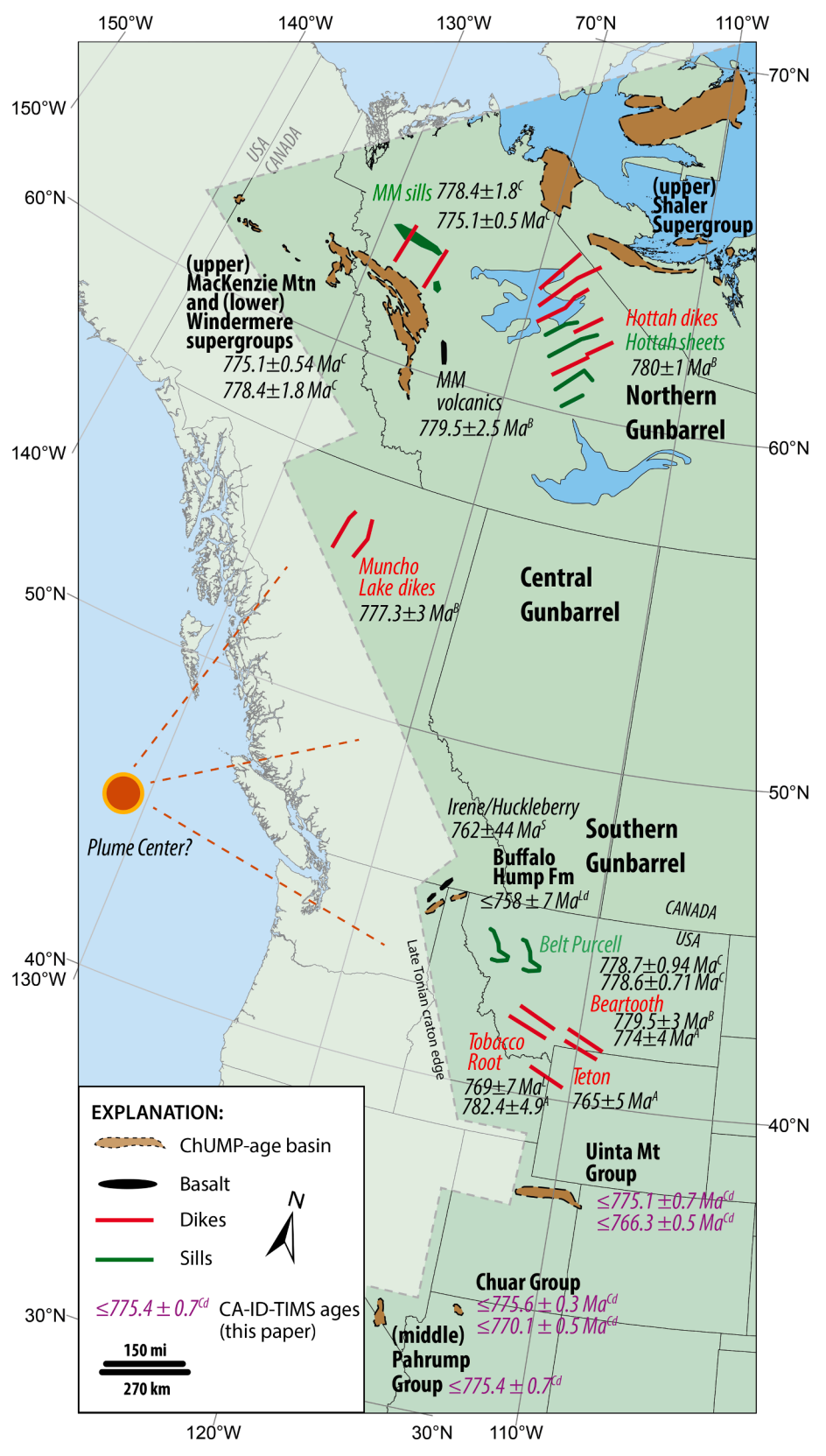


Fig. 1. Outcrop extent of Late Tonian basins in western Laurentia (modern day coordinates) and related igneous sources of the Gunbarrel Large Igneous Province (GLIP). New CA-ID TIMS ages indicate ChUMP basins of the SW US initiated ca. < 775-<766 Ma (this paper). The correlative Buffalo Hump Formation and Coates Lake Group (and equivalents) do not have basal unit ages, but geochronology suggests they are generally within the same age range (ca. (780). Collectively, these greater 'ChUMP basins' constrain early continental extension of Rodinia. Detrital sources for zircons could be entirely from the Gunbarrel Large Igneous Province, yet no felsic igneous rocks have been identified. For ages of Gunbarrel igneous rocks, see Jefferson and Parrish 1989; Harlan et al., 1997; Milton et al., 2017; Mackinder et al., 2019 and references therein. Plume center placement from Mackinder et al., (2019). MM = MacKenzie Mountains. Exponent abbreviation on ages: Cd = CA-ID TIMS U-Pb detrital zircon: C = CA-ID TIMS U-Pb igneous zircon; Ld-LA ICPMS U-Pb detrital zircon; L = LA ICPMS U-Pb igneous zircon; B = U-Pb baddeleyite; A = Ar-Ar; S = Sm-Nd. B = Beartooth and Teton Mountains; BP = Belt Purcell and Tobacco Root Mountains. Rift margin model (cratonic edge) from Macdonald et al., (2023).

2003; Dehler et al., 2017; Dehler, 2014; Porter, 2016; Porter and Riedman, 2016; Morais et al., 2019; Riedman et al., 2021); 3) a record of meter-scale facies repetitions interpreted to exhibit Milankovitch cyclicity (Chuar Group; Dehler et al., 2001), and, 4) large-scale variability in  $\delta^{13}C_{org}$  and  $\delta^{13}C_{dol}$  -isotope values that have been attributed to varying rates of local and global carbon burial across Laurentia (Dehler et al., 2017; Strauss et al., 2015; Smith et al., 2016; Dehler et al., 2017).

Nonetheless, the previously published laser ablation-inductively coupled mass spectrometry (LA-ICP-MS) detrital zircon U-Pb maximum depositional ages (MDAs) for the basal ChUMP units possess errors in excess of 1 % (Fig. 3; Dehler et al. 2010, Mahon et al., 2014a, Mahon et al., 2014b, Dehler et al., 2017), saddling these maximum ages with up to tens of millions of years of uncertainty. Here we apply more precise and accurate geochronology using U-Pb chemical abrasion-

isotope dilution-thermal ionization mass spectrometry (CA-ID-TIMS) of youngest grain populations identified by LA-ICP-MS to further test the conceptual model of a regionally expansive system of intermittently connected epicratonic basins, or the "ChUMP seaway hypothesis" (Dehler et al., 2017; Bullard, 2018), including the evaluation of ChUMP correlatives farther north along the western margin of Laurentia (Fig. 1, Strauss et al., 2015; Brennan et al., 2021) and on potential conjugate margins (e.g., Mulder et al., 2018). With these new ages on the already well dated Chuar Group, this paper culminates with a Bayesian model of the Chuar Group and its implications for late Tonian Earth History.

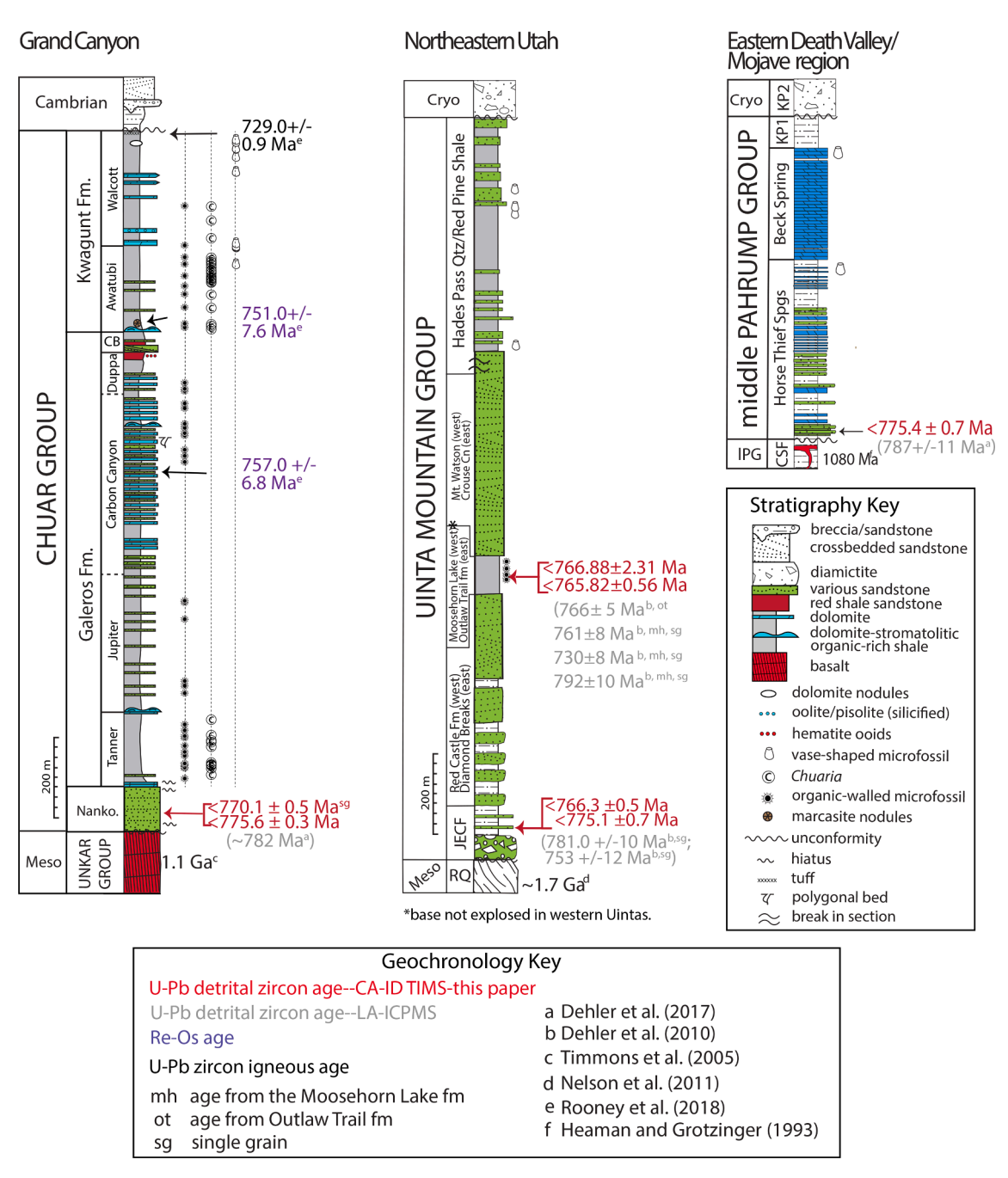


Fig. 2. ChUMP stratigraphic columns showing first-occurrence of vase-shaped microfossil, and organic-walled microfossil and Chuaria distribution (see S1) along with previous and updated geochronology (S2-S4, this study). The Mineral Fork Formation is extrapolated from relationships with the Big Cottonwood Formation to the west (see Dehler et al., 2010). Modified from Dehler et al., (2017).

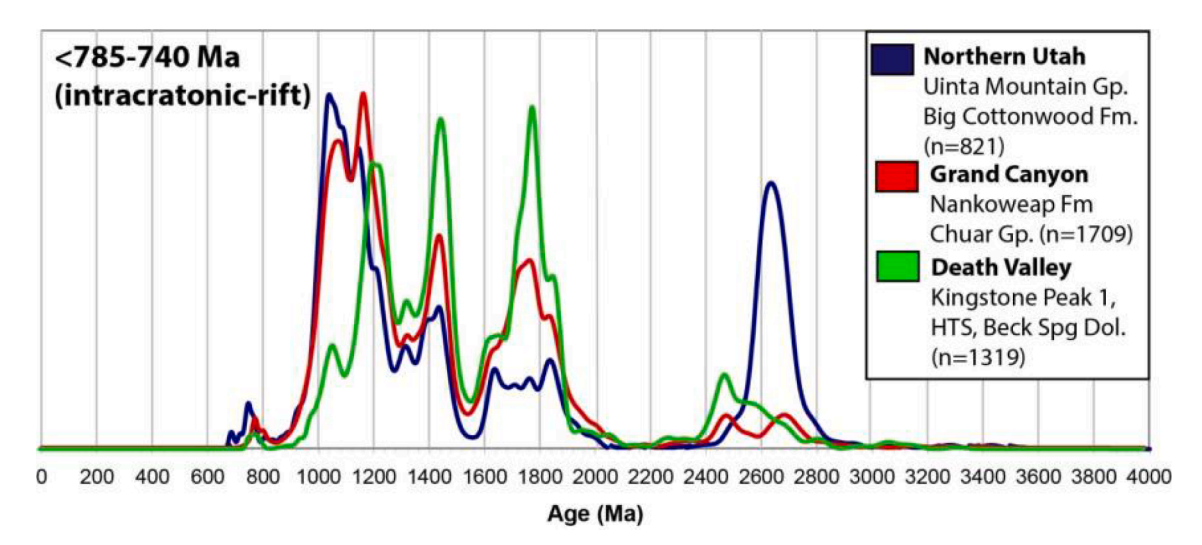


Fig. 3. Detrital zircon probability density plot modified from Dehler et al., 2017. The plot shows the distribution of detrital zircon U-Pb LA-ICP MS ages found in the Uinta Mountain Group (blue), the Chuar Group (red), and the Pahrump Group (green). Note that these previously published LA-ICP-MS detrital zircon U-Pb maximum depositional ages for the basal ChUMP units possess errors in excess of 1 %. The peaks at ~780 Ma that occurs in samples from all three of the ChUMP units prompted this study and are now more accurately dated as ca. 766 to 776 Ma in all three basins.

#### 2. Previous geochronology

#### 2.1. Chuar Group, Grand Canyon, Arizona

Previous work constrained the deposition of the Chuar Group from < 782 Ma to 729.0  $\pm$  0.9 Ma (Dehler et al., 2017; Rooney et al., 2018). Dehler et al. (2017) identified 11 detrital zircon grains from the Nankoweap Formation (basal Chuar unit) ranging in age from 763  $\pm$  21 to 832  $\pm$  13 Ma with an interpreted maximum depositional of  $\sim$ 782 Ma (Fig. 3). Rooney et al. (2018) obtained a Re-Os age of 757.0  $\pm$  6.8 Ma from organic-rich carbonates of the Carbon Canyon Member, and Awatubi Member marcasite nodules yielded an age of 751.0  $\pm$  7.6 Ma. These marcasite nodules also yielded an Ar-Ar age of 764  $\pm$  8 Ma (Dehler et al., 2017). A CA-ID-TIMS U-Pb zircon age of 729.0  $\pm$  0.9 Ma on a volcanic ash bed in the uppermost Walcott Member (Rooney et al., 2018) constrains deposition at the top of the Chuar Group (previously 742  $\pm$  6 Ma in Karlstrom et al., 2000) (Fig. 2).

#### 2.2. Uinta Mountain Group, northern utah

Dehler et al. (2010) reported a U-Pb detrital zircon maximum depositional age of 766.4  $\pm$  4.8 Ma from the Outlaw Trail formation (sample SCUMG-9) of the lower-middle Uinta Mountain Group (UMG) of the eastern Uinta Mountains based on U-Pb detrital zircon SHRIMP (Sensitive High-Resolution Ion Microprobe) analyses. Detrital zircons younger than 800 Ma were also identified using U-Pb LA-IC-PMS in the basal Jesse Ewing Canyon Formation (sample 91PL05) of the eastern Uinta Mountains, with ages of 781  $\pm$  10 Ma and 753  $\pm$  12 Ma, and the Moosehorn Lake formation (sample 73PL05) of the lower-middle UMG, western Uinta Mountains, with zircons as young as 792  $\pm$  10 Ma, 761  $\pm$  8 Ma, and 730  $\pm$  8 Ma (Fig. 3; Dehler et al. 2010). The Moosehorn Lake formation is the lowest unit in the western Uinta Mountains and the base is not explosed there.

# 2.3. Middle Pahrump Group, Death Valley California

Mahon et al. (2014a), Mahon et al. (2014b) presented a maximum depositional age of 787  $\pm$  11 Ma for the basal Horse Thief Springs Formation (HTS) based on LA-ICP-MS U-Pb detrital zircon analyses of Neoproterozoic grains (n = 6) across four samples (Fig. 3; 4d). Two "young" (Neoproterozoic) grains each were recovered from samples K03DV10 (786  $\pm$  19 Ma and 760  $\pm$  6 Ma) and K03DV11 (802  $\pm$  11 Ma

and 785  $\pm$  11), which were taken < 12 m above the unconformity with the underlying Crystal Spring Formation at the Saratoga Springs locality. Samples 12RMSS5 (same locality as K03DV10 and K03DV11) and 4CD11 (unit F of the Horse Thief Springs Formation in the Kingston Range) each contained single "young" grain ages of 780  $\pm$  17 and 774  $\pm$  10 Ma, respectively. Mahon et al. (2014a), Mahon et al. (2014b) found the weighted mean of ages for these grains to be 775  $\pm$  18 Ma. With an outlier excluded, they acquired a mean age of 787  $\pm$  11 Ma as a more conservative estimate for the maximum depositional age of the HTS (Mahon et al., 2014a; Mahon et al., 2014b).

#### 3. Methods

# 3.1. Sample acquisition

Where available, late Tonian zircon grains were plucked from mounts previously analyzed via LA-ICP-MS at University of Arizona's Laserchron Facility ("legacy mounts", Mahon et al., 2014a, Mahon et al., 2014b; Dehler et al. 2017; unpublished data). To supplement this small sample pool of Neoproterozoic zircons within the ChUMP legacy mounts, additional archived rock samples were mechanically and chemically separated and analyzed using LA-ICP-MS at Boise State University. We further sampled a different, finer-grained arkosic sandstone facies in the Jesse Ewing Canyon Formation with the hope of augmenting the existing, small population of Neoproterozoic zircon found in the original Jesse Ewing Canyon Formation mount (Dehler et al., 2010).

Three legacy mounts from the Nankoweap Formation (Dehler et al., 2017) were used (CDGC5, CDGC6, NAN-1; quartz arenite) and one new mount (CDGC4; quartz arenite) was made. All samples are from within a measured section in Nankoweap Canyon (Dehler et al., 2017; Table 1; S5).

Two legacy mounts from the UMG (unpublished data) were used: one from the Moosehorn Lake formation (MH6-23-08; quartz arenite), and one from the Outlaw Trail formation (OTDZ-1; subfeldspathic arenite). A mount was made for a new sample, CMD17-JECF-5, from a similar stratigraphic interval and facies as the Jesse Ewing Canyon Formation (91PL05) sample from Dehler et al (2010) near the base of the unit (S6).

Two legacy mounts from the Horse Thief Springs Formation (Mahon et al., 2014a, Mahon et al., 2014b) were used along with three new mounts. Sample 12RMSS-5 (white quartzite) is from the basal Horse Thief Springs Formation, Saratoga Springs, Death Valley, and is known



Fig. 4. Facies sampled for detrital zircon geochronology in this and previous related studies. A. Trough-crossbedded quartz arenite Nankoweap Formation, Chuar Group; subfeldsarenite hummocks and laminations, Jesse Ewing Canyon Formation, UMG; siltstone and fine-grained subfeldsarenite, Outlaw Trail formation, UMG; D. meter-scale lenticular bodies of fine-grained quartz arenite, Moosehorn Lake Formation, UMG; and E. Trough-cross bedded quartz arenite, basal Horse Thief Springs Formation, Pahrump Group.

to contain late Tonian grains (Mahon et al., 2014a, Mahon et al., 2014b). A legacy mount was used and three new mounts were made of this sample. The other Horse Thief Springs Formation legacy mount, 4CD11, is from a silty quartz arenite (F-unit) taken at the Horse Thief Springs -Beck Spring contact, Kingston Range (S7; Maud, 1979).

#### 3.2. Sample preparation

Heavy minerals were separated from hand samples by conventional density and magnetic methods. All prepared zircon separates were placed in a muffle furnace at 900 °C for 60 h in quartz beakers to anneal minor radiation damage; annealing enhances cathodoluminescence (CL) emission (Nasdala et al., 2002), promotes more reproducible interelement fractionation during LA-ICP-MS (Allen and Campbell, 2012), and prepares the crystals for subsequent chemical abrasion (Mattinson, 2005).

Both random and non-random samplings of zircons were taken for each sample being re-analyzed. For random sampling, grains were coated on one side of  $1\times15$  mm strips of double-sided Kapton tape, which were affixed to a larger surface of double-sided tape. For the non-random sampling, we searched for grains that were euhedral, which indicate that they have been eroded less during their transport history and are therefore more likely to be young. These grains were hand-picked, sized, and laid out in rows on double-sided tape. Both types of samples were then prepared as 1 cm diameter cold-mounted two-part epoxy mounts, ground to the average center of grains, and polished with SiC lapping film and  $0.3~\mu m$  alumina. The finished mounts were carbon coated and digitally photomicrographed in cathodoluminescence (CL) using a Gatan Mini-CL detector mounted on a JEOL T300 scanning electron microscope. From these compiled images, the location of spot analyses for LA-ICP-MS were selected and recorded.

# 3.3. LA-ICP-MS analysis

LA-ICP-MS analysis at Boise State University utilized an X-Series II quadrupole ICPMS and New Wave Research UP-213 Nd:YAG UV (213 nm) laser ablation system. Analytical methods followed those described in Macdonald et al. (2018), and are summarized in Tables S2-S4. Briefly, in-house analytical protocols, standard materials, and data reduction software were used for acquisition and calibration of U-Pb dates and a suite of high field strength elements (HFSE) and rare earth elements (REE). Zircon was ablated with a 25 µm diameter apertured laser spot using fluence and pulse rates of  $\sim 5$  J/cm<sup>2</sup> and 10 Hz, during a 45 s analysis (15 sec gas blank, 30 sec ablation) that excavated a pit  $\sim$ 25  $\mu m$ deep. Ablated material was carried by a 1.2 L/min He gas stream to the nebulizer flow of the plasma. For concentration calculations, background-subtracted count rates for each analyte were internally normalized to 29Si and calibrated with respect to NIST SRM-610 and -612 glasses as the primary standards. For U-Pb and  $^{207}$ Pb/ $^{206}$ Pb dates, instrumental fractionation of the background-subtracted ratios was corrected and dates were calibrated with respect to interspersed measurements of the primary standard Plešovice zircon (Sláma et al., 2008). Radiogenic isotope ratio and age error propagation for all analyses includes uncertainty contributions from counting statistics and background subtraction. Because the detrital zircon analyses are interpreted individually, uncertainties from the standard calibrations are propagated into the errors on each date (  $\sim\!2$  % (20) for  $^{206}\text{Pb/}^{238}\text{U}$  and  $\sim\!1$  % (20°) for  $^{207}\text{Pb}/^{206}\text{Pb}$ ).

# 3.4. CA-ID-TIMS analysis

U-Pb geochronology methods for isotope dilution thermal ionization mass spectrometry follow those previously published by Macdonald et al. (2018). All analyses were undertaken on crystals previously mounted, polished and imaged by CL, and analyzed by LA-ICP-MS. Zircon crystals were subjected to a modified version of the chemical

**Table 1**Detrital zircon sample localities and sources.

ChUMP unit	Sample name	Formation	Litho.	Locality	UTM coordinates	References
Chuar	CDGC4	Nankoweap Fm	Quartz	Nankoweap Can.	12S 0,419,918	Dehler et al 2017
		Grand Can	arenite	Grand Canyon	4,015,852	
Chuar	CDGC5	Nankoweap Fm	Quartz	Nankoweap Can.	12S 0,419,918	Dehler et al 2017
		Grand Can	arenite	Grand Canyon	4,015,852	
Chuar	CDGC6	Nankoweap Fm	Quartz	Nankoweap Can.	12S 0,419,918	Dehler et al 2017
		Grand Can	arenite	Grand Canyon	4,015,852	
Chuar	NAN1	Nankoweap Fm	Quartz	Nankoweap Can.	12 T 0,504,138	Dehler et al 2017
		Grand Can.	arenite	Grand Canyon	4,498,612	
UMG	6-23-8-2	Moosehorn	Quartz	Slate Gorge	12 T 0,504,230	This paper
		Lake fm	arenite	W. Uintas	4,498,284	
UMG	OTDZ-1	Outlaw Trail fm	Sub	Browns Park	12 T 652,199	Rybczynski 2009; Dehleret al., 2010
			arkose	E. Uintas	4,526,544	
UMG	17CMD-JEC-5	Jesse Ewing	Arkose	Browns Park	12 T 657,129	This paper
		Canyon Fm		E. Uintas	4,532,100	
Pahrump	12RMSS5	Horse Thief	Qtzite	Saratoga Springs	118 0,552,634	Mahon et al 2014
		Springs Fm		DeathValley	3,949,335	
Pahrump	4CD11	Horse Thief Springs Fm	Quartz	Crystal Spring	11S 06,030,506	Mahon et al 2014
			arenite	Kingston Rg	3,949,335	

abrasion method of Mattinson (2005), whereby single crystal fragments plucked from grain mounts were individually abraded in a single step with concentrated HF at 190 °C for 12 h. U-Pb dates and uncertainties for each analysis were calculated using the algorithms of Schmitz and Schoene (2007) and the U decay constants of Jaffey et al. (1971). Uncertainties are based upon non-systematic analytical errors, including counting statistics, instrumental fractionation, tracer subtraction, and blank subtraction. These error estimates should be considered when comparing our <sup>206</sup>Pb/<sup>238</sup>U dates with those from other laboratories that used tracer solutions calibrated against the EARTHTIME gravimetric standards. When comparing our dates with those derived from other decay schemes (e.g., 40 Ar/39 Ar, 187 Re-187 Os), the uncertainties in tracer calibration (0.03 %; Condon et al., 2015; McLean et al., 2015) and U decay constants (0.108 %; Jaffey et al., 1971) should be added to the internal error in quadrature. Quoted errors for calculated weighted means are thus of the form  $\pm$  X(Y)[Z], where X is solely analytical uncertainty, Y is the combined analytical and tracer uncertainty, and Z is the combined analytical, tracer and <sup>238</sup>U decay constant uncertainty.

#### 3.5. Bayesian age modeling

We used the Bayesian age modeling software *modifiedBchron* (Trayler et al., 2019), an open source R package evolved from the package *Bchron* (Haslett & Parnell, 2008) for deep time applications. These packages are identical in their use of a compound Poisson-gamma distribution of accumulation events under the constraint of stratigraphic superposition to describe the *prior* probability of an ensemble of piece-wise linear sedimentation paths, which are conditioned by *likelihood* functions describing dated horizons (Haslett & Parnell, 2008). Additionally, modifiedBchron uses an adaptive proposal algorithm in its Markov Chain Monte Carlo engine to remove any necessity for user scaling of the space or time domains, and still ensure effective and efficient sampling of the posterior parameter distributions (Trayler et al., 2019).

For the likelihood functions, *modifiedBchron* can represent radioisotopic ages as a single Gaussian normal distribution (for example to represent a weighted mean age) but can also aggregate individual (normally-distributed) crystal analyses of a sample at a given stratigraphic horizon to accurately reflect the complex probability function of dated crystals in some volcanic event beds. Similarly, uniform distributions can be input as likelihood functions (e.g., to represent magnetostratigraphic, chemostratigraphic, or cyclostratigraphic signals), and aggregated at any stratigraphic horizon to approximate any arbitrarily complex distribution, such as arising from detrital zircon MDA constraints. We used this feature to model the detrital zircon horizon in the Nankoweap Formation, with the MDA constrained by the youngest

zircon(s) and the minimum depositional age constrained by the next overlying depositional age, in this case the Re-Os age in the Carbon Canyon member (Rooney et al. 2018).

The full R script and data files necessary to reproduce an ensemble of age models, using different probability functions for the detrital zircon MDA in the Nankoweap Formation, are compiled in Supplementary file S8. The preferred posterior modifiedBchron age model using the youngest detrital zircon MDA (770.1  $\pm$  0.5 Ma) was used to predict the median age and 95 % credible interval for selected horizons of interest with the Chuar Group (Table 3).

#### 4. Results

Of the detrital zircons taken from the mounts of previous studies and generated from new processing of rock from previous field samples, 21 Chuar grains, 10 Uinta Mountain grains, and 12 Pahrump grains were chosen for CA-ID-TIMS analysis and subsequently produced interpretable results via this tandem geochronology (Table 2; S2-4).

Of the 21 grains from the Chuar Group (Nankoweap Formation), four yielded  $^{206}\text{Pb}/^{238}\text{U}$  dates in excess of 1000 Ma (Table 2; Dehler et al., 2017, supplementary material). These uninformative dates could be due to Pb-loss biasing the LA-ICP-MS result to a younger value with respect to the chemically abraded CA-ID-TIMS result, or due to misidentification of grains in legacy mounts. Two resolvably older Tonian grains yielded U-Pb dates of 800.7  $\pm$  0.5 and 778.4  $\pm$  1.1 Ma. Eleven of the 14 remaining grains yielded a large population of ca. 775 Ma zircons with a mode of 775.7  $\pm$  1.0 Ma (20; MSWD = 0.44; Fig. 5). These zircons came from samples CDGC4 and NAN1, 34 m above the base of the unit (S5). Another sample 70 m above the base (CDGC-5; S5), yielded two 775 Ma grains and a single grain at 770.1  $\pm$  0.5 Ma (20). This youngest grain is concordant with precise  $^{206}\text{Pb}/^{238}\text{U}$  and  $^{206}\text{Pb}/^{238}\text{U}$  dates, and therefore we interpret this as a robust estimate of the maximum depositional age of the Nankoweap Formation for subsequent age-depth modeling.

Of the ten grains from the UMG that were analyzed via CA-ID TIMS, one is from the western UMG Moosehorn Lake formation (MH-6–23-8–2; Fig. 2; Fig. 6; S6), from a sample located approximately 1150 m above the base of the exposed UMG (base not exposed west). It yielded a  $^{206} \rm Pb/^{238} U$  date of 766.9  $\pm$  2.3 Ma, which is consistent with the SHRIMP date of 766  $\pm$  5 Ma interpreted by Dehler et al. (2010). An additional three grains were analyzed from the correlative eastern UMG Outlaw Trail formation (OTDZ-1; S6); this sample was collected from ~2,500 m above the base of the UMG. These grains yielded concordant U-Pb analyses with  $^{206} \rm Pb/^{238} U$  dates of 892.8  $\pm$  0.6 Ma, 765.8  $\pm$  0.6 Ma, and 592.0  $\pm$  0.6 Ma (Table 2). The oldest of these exceeds the previously known MDA of the unit, while the youngest zircon provides an

Precambrian Research 396 (2023) 107156

**Table 2** Zircon CA-IDTIMS U-Pb isotopic data.

	Compo <u>Th</u>	sitional Para <sup>206</sup> Pb*	ameters mol %	Pb*	Pbc	<sup>206</sup> Pb	Radiog <sup>208</sup> Pb	enic Isotope	e Ratios	<sup>207</sup> Pb		<sup>206</sup> Pb		corr.	Dates 207Pb		<sup>207</sup> Pb		<sup>206</sup> Pb		Tanden	n LA-ICP 206Pb	MS
Sample	U	$\begin{array}{c} \times 10^{-13} \\ \text{mol} \end{array}$	<sup>206</sup> Pb*	Pb <sub>c</sub>	(pg)	<sup>204</sup> Pb	<sup>206</sup> Pb	<sup>206</sup> Pb	% err	<sup>235</sup> U	% err	<sup>238</sup> U	% err	coef.	<sup>206</sup> Pb	±	<sup>235</sup> U	±	<sup>238</sup> U	±	spot	<sup>238</sup> U	±
(a)	(b)	(c)	(c)	(c)	(c)	(d)	(e)	(e)	(f)	(e)	(f)	(e)	(f)		(g)	(f)	(g)	(f)	(g)	(f)			(f)
Uinta Mountai	in Group,	Outlaw Tra	il formation																				
OTDZ-1-z2	0.255	2.0468	0.9974	108	0.45	6840	0.078	0.06950	0.080	1.4234	0.140	0.14855	0.070	0.926	913	2	898.8	0.8	892.8	0.6	92	783	2
OTDZ-1-z1	0.650	0.7912	0.9962	83	0.25	4776	0.201	0.06486	0.113	1.1286	0.167	0.12620	0.077	0.821	770	2	767.1	0.9	766.1	0.6	24	707	2
OTDZ-1-z3	0.461	0.5899	0.9928	41	0.35	2511	0.143	0.05974	0.199	0.7925	0.253	0.09622	0.104	0.668	594	4	592.6	1.1	592.2	0.6	27	564	2
Uinta Mountai	in Group,	Moosehorn	Lake forma	tion																			
MH6-23-6-z4	0.695	0.0886	0.9591	7.5	0.31	442	0.214	0.06487	1.056	1.1300	1.167	0.12633	0.320	0.470	770	22	767.7	6.3	766.9	2.3	107	705	2
Uinta Mountai	in Group,	Jesse Ewin	g Canyon Fo	rmatio	n																		
17CMD-JEC5 z7	1.461	0.0674	0.9244	4.6	0.46	239	0.450	0.06663	1.704	1.1781	1.896	0.12824	0.556	0.474	826	36	790.4	10	777.8	4.1	L2/ 128	718	4
17CMD-JEC5 z2	1.474	0.1091	0.9562	8.3	0.42	412	0.454	0.06518	0.859	1.1487	0.959	0.12781	0.269	0.492	780	18	776.6	5.2	775.4	2.0	L/334	818	4
17CMD-JEC5 z1	1.161	0.3266	0.9708	12	0.82	610	0.358	0.06509	0.353	1.1465	0.412	0.12774	0.113	0.622	777	7	775.6	2.2	775.0	0.8	L/282	813	3
17CMD-JEC5 z4	0.843	0.1016	0.8839	2.5	1.12	153	0.260	0.06532	1.239	1.1385	1.364	0.12642	0.334	0.480	785	26	771.8	7.4	767.4	2.4	L2/61	735	3
17CMD-JEC5 z3	0.544	0.1344	0.9341	4.3	0.79	271	0.168	0.06442	1.060	1.1220	1.187	0.12632	0.322	0.511	755	22	763.9	6.4	766.9	2.3	L2/49	812	2
17CMD-JEC5 z5	0.568	0.0999	0.9393	4.8	0.54	296	0.175	0.06470	1.093	1.1262	1.202	0.12624	0.284	0.486	765	23	765.9	6.5	766.4	2.0	L2/ 105	736	4
Pahrump Grou	up. Horse	Thief Sprin	gs formation	ı																			
4CD-11-z2	0.573	0.1501	0.9434	5.2	0.75	315	0.170	0.09007	0.581	3.0790	0.757	0.24793	0.404	0.652	1427	11	1427.5	5.8	1427.8	5.2	30	772	9
4CD-11-z3	0.532	0.1339	0.9584	7.1	0.48	433	0.159	0.08461	0.687	2.6222	0.812	0.22478	0.329	0.552	1307	13	1306.9	6.0	1307.1	3.9	66	889	
4CD-11-z1	0.666	0.1312	0.9635	8.4	0.41	495	0.199	0.08440	0.676	2.6038	0.811	0.22374	0.338	0.575	1302	13	1301.7	6.0	1301.6	4.0	27	873	
12RM-SS5-z8	0.478	0.4255	0.9937	48	0.23	2846	0.145	0.07489	0.184	1.8572	0.296	0.17986	0.180	0.808	1066	4	1066.0	2.0	1066.2	1.8	203	1068	2
12RM-SS5-z6	0.402	1.8844	0.9902	30	1.57	1797	0.122	0.07343	0.110	1.7334	0.169	0.17120	0.077	0.856	1026	2	1021.0	1.1	1018.7	0.7	174	998	8
12RM-SS5-z3	1.155	0.7013	0.9579	7.9	2.59	418	0.353	0.06966	0.257	1.4664	0.353	0.15268	0.193	0.703	918	5	916.6	2.1	916.0	1.6	37	917	4
12RM-SS5-z7	0.176	0.5176	0.9951	57	0.21	3719	0.054	0.07216	0.111	1.5019	0.221	0.15096	0.158	0.880	990	2	931.2	1.3	906.3	1.3	212	1001	1
4CD-11-z4	0.577	0.1649	0.9780	14	0.31	820	0.178	0.06814	0.459	1.2547	0.693	0.13355	0.475	0.751	873	10	825.5	3.9	808.1	3.6	98	612	
12RM-SS5-z2	0.538	6.0064	0.9968	94	1.63	5486	0.166	0.06605	0.071	1.2030	0.132	0.13209	0.065	0.965	808	1	802.0	0.7	799.8	0.5	18	823	3
12RM-SS5-z5	1.020	0.0678	0.8916	2.8	0.69	165	0.314	0.06407	2.464	1.1314	2.632	0.12806	0.528	0.409	744	52	768.4	14	776.8	3.9	58	786	3
12RM-SS5-z1	1.008	0.3473	0.9451	5.8	1.70	321	0.311	0.06496	0.449	1.1450	0.523	0.12783	0.171	0.565	773	9	774.9	2.8	775.5	1.3	232	801	2
12RM-SS5-z4	0.908	0.2534	0.9684	10	0.69	566	0.280	0.06509	0.418	1.1471	0.478	0.12781	0.125	0.577	777	9	775.9	2.6	775.3	0.9	94	787	5
Chuar Group,	Nankowe	ap formatio	on																				
CDGC5-z3	0.323	0.4886	0.9946	55	0.22	3349	0.094	0.11394	0.083	5.2568	0.195	0.33461	0.144	0.922	1863	2	1861.9	1.7	1860.7	2.3	31	-	-
CDGC6-z2	0.285	4.5486	0.9761	12	9.26	753	0.087	0.07635	0.134	1.9188	0.188	0.18228	0.074	0.823	1104	3	1087.7	1.3	1079.4	0.7	24	1966	7
CDGC5-z7	0.035	0.5798	0.9951	54	0.24	3654	0.011	0.07566	0.132	1.8964	0.188	0.18180	0.089	0.770	1086	3	1079.8	1.3	1076.8	0.9	79	-	-
CDGC5-z4	0.434	0.0635	0.9569	6.6	0.24	418	0.132	0.07456	0.973	1.8466	1.156	0.17962	0.501	0.552	1057	20	1062.2	7.6	1064.9	4.9	39	-	-
CDGC6-z1	1.818	0.9311	0.9943	70	0.45	3144	0.560	0.06585	0.127	1.2007	0.178	0.13225	0.071	0.815	802	3	800.9	1.0	800.7	0.5	5	794	7
K12-CDGC4- z10	0.922	0.3037	0.9781	15	0.56	822	0.284	0.06526	0.373	1.1548	0.439	0.12834	0.145	0.581	783	8	779.5	2.4	778.4	1.1	311	759	4
K12-CDGC4- z6	1.001	0.1690	0.9408	5.4	0.89	300	0.308	0.06511	0.683	1.1492	0.762	0.12801	0.183	0.527	778	14	776.8	4.1	776.5	1.3	598	805	4

(continued on next page)

- (a) z1, z2 etc. are labels for zircon fragments annealed and chemically abraded after Mattinson (2005).
- (b) Model Th/U ratio iteratively calculated from the radiogenic 208Pb/206Pb ratio and 206Pb/238U age.
- (c) Pb\* and Pbc represent radiogenic and common Pb, respectively; mol % <sup>206</sup>Pb\* with respect to radiogenic, blank and initial common Pb.
- (d) Measured ratio corrected for spike and fractionation only; all samples spiked with the ET535 tracer. Fractionation estimated at 0.18+/-0.03 %/a.m.u. for Pb analyses, based on analysis of ET2535 spike samples over the same experimental period.
- (e) Corrected for fractionation, spike, and common Pb; up to 0.5 pg of common Pb was assumed to be procedural blank:  $206Pb/204Pb = 18.042 \pm 0.61$  %;  $207Pb/204Pb = 15.537 \pm 0.52$  %;  $208Pb/204Pb = 37.686 \pm 0.63$  % (1-sigma), with the rest assigned to initial common Pb, using the Stacey and Kramers (1975) two-stage Pb isotope evolution model at the nominal sample age.
- (f) Errors are 2-sigma, propagated using the algorithms of Schmitz and Schoene (2007).
- (g) Calculations based on the decay constants of Jaffey et al. (1971). 206Pb/238U and 207Pb/206Pb ages corrected for initial disequilibrium in 230Th/238U using Th/U[magma] = 3.

**Table 3**Results of Bayesian age modeling.

Height	Quantile	Quantiles — age (Ma)										
(m)	2.5 %	50 %	97.5 %	Event								
Chuar Group (Grand Canyon, USA)												
1719	727.93	728.93	729.81	Top Walcott								
1718	728.09	728.98	729.85	Walcott Tuff; U-Pb zircon (729.0 $\pm$								
				0.9 Ma)								
1447	732.95	739.57	745.91	Cycliocyrillium								
1438	733.12	739.92	746.12	Base Walcott								
1416	733.57	740.75	746.63	FO VSMs								
1368	734.75	742.57	747.88	LO C. globosa								
1343	735.52	743.52	748.65	LO L. laufeldi								
1319	736.41	744.43	749.48	FO VSMs, no image								
1232	741.89	748.13	753.24	Re-Os marcasite (751.0 $\pm$ 7.6 Ma)								
1227	742.14	748.35	753.47	Base Awatubi								
1180	743.90	749.74	754.87	Base Carbon Butte								
1115	745.99	751.44	756.32	Base Duppa								
996	749.07	754.48	759.12	Baicalia								
896	752.17	757.30	762.42	Re-Os A1407 (757.0 $\pm$ 6.8 Ma)								
561	755.45	760.68	765.97	Base Carbon Canyon								
371	757.47	763.80	767.91	LO Valeria lophostriata								
296	758.10	764.70	768.40	Base Jupiter								
158	759.36	766.40	769.38	FO L. laufeldii								
111	759.89	767.02	769.79	Base Tanner								
34	761.15	768.35	770.72	U-Pb detrital zircon CDGC5 (≤7								
0	761.80	769.16	777.69	Base Nankoweap Fm								

anomalous age within the Ediacaran, which we reject as a contaminant (Table 2). The third analysis of 765.8  $\pm$  0.6 Ma, however, mimics the result from the western UMG Moosehorn Lake formation.

The remaining six UMG grains, from  ${\sim}60$  m above the base of the Jesse Ewing Canyon Formation in the eastern Uinta Mountains, yielded two distinct age modes comprising three grains each (Fig. 2; 6; Table 2; S6). The older mode of 775.1  $\pm$  1.2 Ma is very similar to the dominant Tonian detrital zircon mode of the Nankoweap Formation. The younger mode is 766.3  $\pm$  0.9 Ma, consistent with the single detrital zircons in the Moosehorn Lake formation and Outlaw Trail formation. The presence of this younger population in the basal strata of the eastern UMG demands that the entire UMG is younger than 766 Ma.

In the Pahrump Group, four of the 12 analyzed Horse hief Springs formation (HTSF) grains are from the Kingston Range (4CD11), and were collected  $\sim\!300$  m above the base. Three of them yielded old  $^{206} \rm Pb/^{238} U$  ages from 1427–1301 Ma, and the fourth grain yielded a

slightly discordant age of 808.1  $\pm$  3.6 Ma. The eight remaining Horse Thief Springs formation grains came from the lower succession at Saratoga Spring (12RMSS5), from a sample 12.5 m above the basal unconformity. Four of these yielded older  $^{206}\text{Pb}/^{238}\text{U}$  ages of 1066 Ma–906 Ma (Table2; Mahon et al., 2014a, Mahon et al., 2014b, supplementary material). The remaining four grains yielded concordant  $^{206}\text{Pb}/^{238}\text{U}$  ages of 799.8  $\pm$  0.5 Ma, 776.8  $\pm$  3.9 Ma, 775.5  $\pm$  1.3 Ma, and 775.3  $\pm$  0.9 Ma. The last three define a mode with a  $^{206}\text{Pb}/^{238}\text{U}$  age of 775.4  $\pm$  1.2 Ma (20; MSWD = 0.28; n = 3) (Fig. 7).

#### 5. Discussion and implications

#### 5.1. Refined detrital zircon geochronology of basal ChUMP units

Fig. 5 demonstrates the increase in accuracy and precision obtained by analyzing zircons from the Nankoweap Fm samples formerly analyzed by LA-ICP-MS with CA-ID-TIMS. Many of our CA-ID-TIMS ages were obtained from grains originally analyzed in the previous study (Dehler et al., 2017). The ages and errors associated with each grain previously left tens of millions of years in which these zircons could have formed. In addition to the improvement in precision associated with isotope dilution measurement, it is important to emphasize the improved accuracy of these measurements. This improvement in accuracy is attributable in part to the application of chemical abrasion treatment, which is highly effective at removing Pb-loss bias (Mattinson, 2005). Improvement in accuracy is also the result of the more rigorous assessment of concordance that can be achieved with the precision of isotope dilution measurements; we can readily assess concordance, and therefore accuracy at the limiting resolution of the <sup>207</sup>Pb/<sup>235</sup>U dates of ca. 1 to 4 Ma. The result is that maximum depositional ages can be confidently assessed and interpreted even on the basis of single grain CA-ID-TIMS analyses, and without the statistical grouping assumptions common to LA-ICPMS treatments (Coutts et al., 2019; Herriott et al., 2019; Vermeesch, 2021). All of the CA-ID-TIMS ages for the Nankoweap Formation (Fig. 5) are precise and concordant, with the stratigraphically lower sample yielding a mode at 775.7  $\pm$  1.0 Ma (n = 11). The stratigraphically higher sample yielded two 775 Ma grains and a single grain at 770.1  $\pm$  0.5 Ma (2 $\sigma$ ). The precision and concordance of this 770 Ma grain objectively refines and supersedes the ca. < 782 LA-ICP-MS maximum depositional age reported by Dehler et al. (2017) for the Nankoweap Fm. of the Chuar Group.

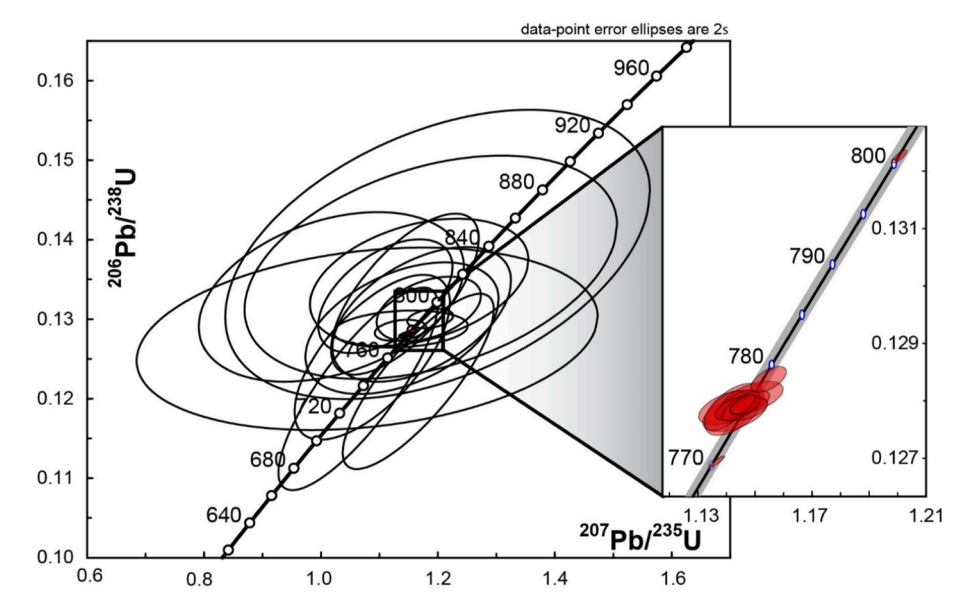


Fig. 5. Chuar (Nankoweap Fm-CDGC4, CDGC5, and NAN1) U-Pb concordia plot. White ellipses indicate LA-ICP MS ages. Red ellipses indicate the twelve refined CA-ID TIMS ages. Note single concordant age at ca. 770 Ma.

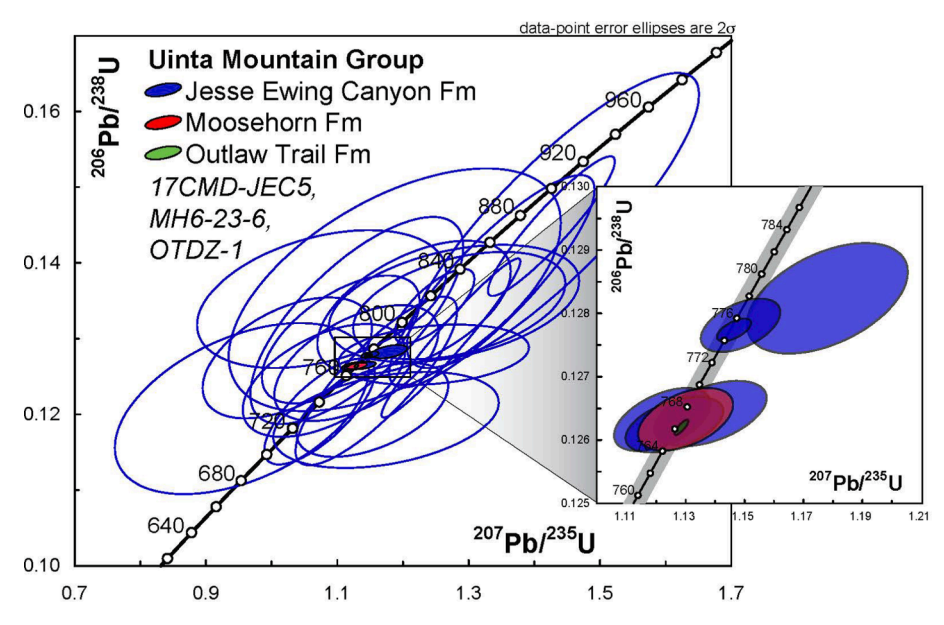


Fig. 6. Uinta Mountain Group U-Pb concordia plot. White ellipses indicate LA-ICP-MS ages. Colored ellipses indicate the refined CA-ID TIMS ages. See key for specific formations and samples that are represented in this plot. The ca. 766 Ma population is found in the lowermost UMG and in the middle UMG, suggesting this is a provenance signature.

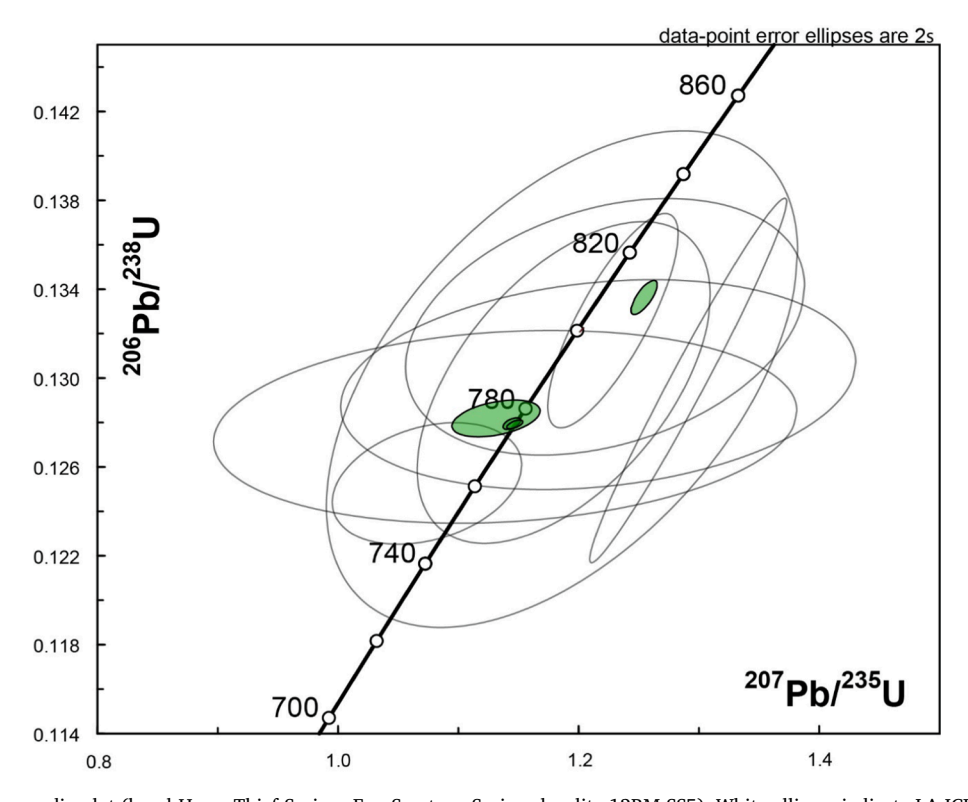


Fig. 7. Pahrump U-Pb concordia plot (basal Horse Thief Springs Fm, Saratoga Springs locality-12RM-SS5). White ellipses indicate LA-ICP-MS ages. Green ellipses indicate the four refined CA-ID TIMS ages.

The new sample from the Jesse Ewing Canyon Formation, Uinta Mountain Group yielded two Tonian detrital zircon age groups (Fig. 6). The older of the two groups has a mode of 775.1  $\pm$  0.7 (n = 3), also identical within error to the  $\sim\!\!775$  Ma detrital zircons from the Nankoweap Fm. However, the other group from the Jesse Ewing Canyon Formation has a resolvable younger mode of 766.3  $\pm$  0.05 Ma (n = 3). This is very important because the younger population revises the MDA for Jesse Ewing Canyon Formation deposition and the Uinta Mountain Group basin initiation to be significantly younger than previously

thought (cf. Dehler et al., 2010). The 766 Ma population is also present several kilometers above the base of the UMG, suggesting a long-lived, reworked 766 Ma source, rapid deposition, and(or) the depositional age of the UMG could be significantly younger than 766 Ma.

One sample from the Horse Thief Springs Fm of the Pahrump Group yielded precise and concordant CA-ID-TIMS ages with a 775.4  $\pm$  0.7 Ma mean age, also identical and within error to the 775 Ma grains in the Nankoweap Formation and the Jesse Ewing Canyon Fm. Thus, there was clearly a common source of 775 Ma sediment available to the ChUMP

basins during their initiation. This CA-ID-TIMS age for the HTS refines and supersedes the  $787 \pm 11$  Ma LA-ICP-MS maximum age reported by Mahon et al. (2014a), Mahon et al. (2014b) for the basal Horse Thief Springs Formation (Fig. 7).

This study demonstrates how tandem CA-ID-TIMS dating of grains that have already been analyzed via LA-ICP MS can vastly improve the precision and accuracy of the interpreted maximum depositional age. ~4,500 zircons were analyzed during the course of the precursor studies to this project (Dehler et al., 2010; Mahon et al., 2014a, Mahon et al., 2014b; Dehler et al., 2017). Using CA-ID-TIMS to re-analyze a specific population of zircons, in this case the few dozen that had already provided the "young" ages in their respective studies, enabled us to refine the maximum depositional age for the ChUMP strata with a precision and accuracy the previous studies lacked (Bullard, 2018).

#### 5.2. Igneous sources for 775 Ma, 770, and 766 Ma Neoproterozoic zircon

Felsic igneous deposits of this age are rare in Western North America, with the exception of a 777 + 2.5/-1.8 Ma (U-Pb zircon LA-ICPMS) faultbounded quartz diorite plug in the MacKenzie Mountains (Jefferson & Parrish 1989). However, there is an extensive array of ca. 775 Ma mafic bodies, collectively known as the Gunbarrel Magmatic event or Gunbarrel Large Igneous Province, some of which have an evolved composition containing zircon (e.g., Harlan, 1993; Harlan et al., 1997; Milton et al., 2017; Mackinder et al., 2019). A zircon-bearing diabase from the Little Dal Basalts yielded a 775.1  $\pm$  0.5 age, which is within [highprecision] error of the ChUMP detrital ages (e.g.; 775.1  $\pm$  0.5; Fig. 1; Milton et al 2017). Considering the overall age and proximity of the Gunbarrel Large Igneous Province, especially the Southern GunBarrel to the UMG basin, along with paleogeographic models (e.g., Dehler et al., 2010), it is permissible that all of the ChUMP basins received 775 to 770 Ma grains from the Gunbarrel Large Igneous Province. The geochemistry of the 775 to 770 grains in the ChUMP sandstones is suggestive of a mafic igneous source as their compositions lie within the mantle zircon array on the U/Yb – Nb/U discriminant diagram of Grimes et al. (2015) (Fig. 8). Interestingly, the composition of the sandstones (feldspathic arenite, quartz arenite (e.g., Dehler et al., 2010), do not represent the

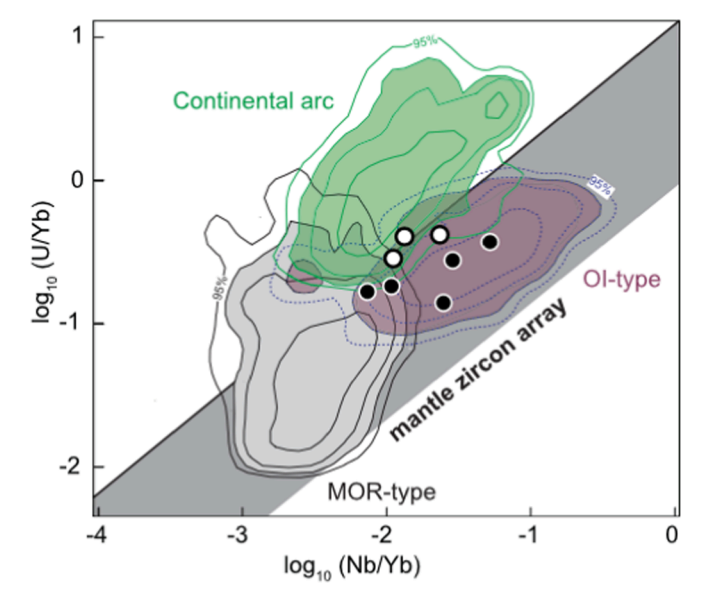


**Fig. 8.** U/Yb-Nb/Yb discriminant diagram of Grimes et al. (2015) illustrating compositional contrast between zircon crystals derived from felsic-intermediate continental arc magmas versus mafic oceanic magmas. Shaded fields are contoured (50–80-90–95 %) two-dimensional kernel density distributions of three compositional groups: Continental arc, OI – ocean island; MOR – mid-ocean ridge. Tonian ChUMP detrital zircons dated by CA-ID-TIMS are illustrated as filled circles (ca. 775 Ma grains) or open circles (ca. 766 Ma grains).

composition of the Gunbarrel outcrops today, suggesting that there was significant reworking of these zircons and (or) they were far traveled.

The source for the 766 Ma grains is less clear. There are no known felsic sources of this age in the region, nor are there mafic sources in the region that have been precisely dated to 766 Ma (Fig. 1; see MacKinder et al., 2019). Interestingly, the detrital zircons from the Buffalo Hump Formation of eastern Washington yielded an age of 758  $\pm$  7 Ma (U-Pb, LA-ICP-MS; 21 grains), which is within [low-precision] error of the 766 Ma population (Brennan et al., 2021). There could simply be a zirconbearing source within the region that has yet to be recognized, is buried, or no longer preserved. Another possible source area for the younger zircon population that is allowable with late Tonian paleogeography and *trans*-continental drainage systems is from the Mount Rogers Formation of the Central and Southern Appalachians, where rhyolite flows yield a U-Pb zircon igneous age of 758  $\pm$  12 Ma (LA-ICPMS, Aleinikoff et al., 1995; Dehler et al., 2010).

Igneous zircon-bearing sources from potential conjugate margins could also have contributed to these age populations. Ding et al. (2021) suggested that North China and Tarim blocks formed conjugate plates to western Laurentia within Rodinia based paleomagnetic data and a reconstruction that ca. 775 Ma dikes in the North China Craton and the ca. 775 Ma Gunbarrel dikes in Laurentia (Mackinder et al., 2019, and references therein) could have formed a radiating LIP. The possibility that the South China block was a conjugate to western Laurentia (modern day coordinates) as part of the "missing link" Rodinia rifting model (Li et al., 2008; Li et al., 2013), has been weakened by geologic evidence (Cawood et al., 2018) and by paleomagnetic studies (Park et al., 2021) that show that South China and Laurentia were at different latitudes ca. 800 Ma (Xian et al., 2020; Jing et al., 2021). Other conjugate margin candidates include Tasmania (Mulder et al., 2020) where there is a 760  $\pm$  12 Ma (Pb-Pb zircon) granite and an altered granitoid with a magmatic age of 777  $\pm$  7 Ma (Pb-Pb zircon; Turner et al., 1998). More general Australian sources remain possible especially if ash fall zircons from Neoproterozoic arc magmatism are considered.

#### 5.3. Correlations between ChUMP-age strata along the western cordillera

Recent geochronologic constraints from the western margin of Laurentia, including this study, elucidate late Tonian correlations (Fig. 9). The high precision ages at the base of the ChUMP units constrain the age of basin formation for the southwestern margin to be younger than or equal to 775-766 Ma. The tuff age at the top of the Chuar Group is the best datum for ChUMP correlation in western Laurentia at 729.0  $\pm$  0.9 Ma. The Buffalo Hump Formation, of NE Washington, contains a detrital zircon provenance signature and an LA-ICP-MS MDA of 758  $\pm$  7 Ma similar to that of the ChUMP strata (Brennan et al., 2021). The Callison Lake Dolostone and correlative Coates Lake Group, Yukon share similar microfossil assemblages and ages of > 752.7  $\pm$  5.5; 739.9  $\pm$  6.5 Ma; and  $732.2 \pm 3.9$  Ma, respectively (Re Os; Strauss et al., 2015). Similarly, the upper Shaler Supergroup, Victoria Island likely contains correlative strata, especially including the upper Wynniatt (Re-Os age of 761  $\pm$  41 Ma), along with the overlying Kilian and Kuujjua formations (which are overlain by the Natkusiak Basalt at 723 Ma + 4/-2 Ma; ID-TIMS U-Pb baddeleyite/zircon age). The caveat with correlations beyond the original ChUMP basins is that most existing geochronology is of lower resolution. Future work is needed to fine tune our understanding of the temporal nature of these units to understand this initial rift phase of Rodinia breakup along Laurentia's western margin.

# 5.4. Bayesian age models for the Chuar Group: Implications for sediment accumulation rates, biology and climate change

Although the detrital zircon age on the Nankoweap Formation obtained for this publication is strictly a maximum depositional age of  $\leq$  770 Ma, this result provides a strong constraint on age models for the lower Chuar Group. The detrital zircon MDA can be incorporated into a

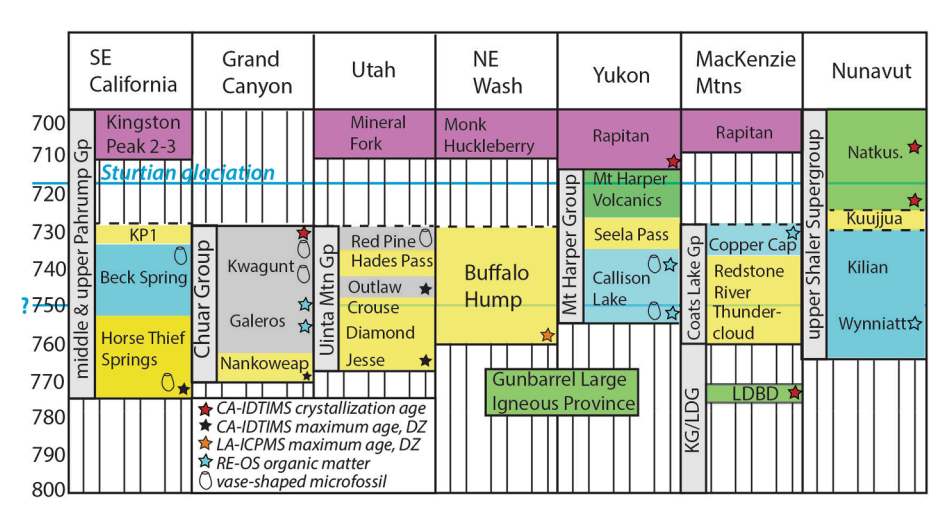


Fig. 9. Wheeler diagram of Late Tonian basins in western Laurentia (modern day coordinates) and related igneous sources of the Gunbarrel Large Igneous Province (GLIP). Note CA-ID TIMS ages indicate basal ChUMP basins of the SW US initiated ca. < 775-<766 Ma (this paper). Yellow = sandstone, blue = carbonate, green = volcanics, grey = shale; and purple = diamictite. LDBD-Little Dal Basalts. Jesse-Jesse Ewing Canyon Fm, Diamond-Diamond Breaks fm, Crouse-Crouse Canyon fm, Outlaw-Outlaw Trail fm (equivalent to west is Moosehorn Lake fm., Hades Pass-Hades Pass Quartzite, Red Pine-Red Pine Shale; KP1-Kingston Peak 1;, DZ-detrital zircon. References: see Strauss et al., 2015; Brennan et al., 2020; Box et al., 2020 and references therein.

Bayesian modeling framework as a conditioning likelihood that assigns uniform probability between the MDA and the age of the next overlying dated horizon. Additional age constraints are derived from Re-Os whole rock and marcasite nodule depositional ages, and the U-Pb zircon age of the tuff in the upper Walcott Member (Rooney et al., 2018). The resulting models quantify the likely sediment accumulation rates throughout the Chuar Group within a continuous age model. The application of a continuous age modeling algorithm is warranted given the lack of evidence for profound unconformities in the Chuar Group. This assumption is also mitigated by the near-unconformity like behavior that can result from *modifiedBchron* compound Poisson-gamma accumulation prior and associated interpolated accumulation paths. Thus limits on the duration of hiatuses in deposition are captured in the 95 % credible interval of the resulting ensemble of models.

Whereas little change in sediment accumulation rate was indicated by the previously published LA-ICP-MS detrital zircon MDA (782.4  $\pm$  6.8 Ma; Dehler et al., 2017), our new CA-ID-TIMS MDAs necessitate a change in subsidence and sediment accumulation rates throughout Chuar time (Fig. 10). Early deposition of the Nankoweap and Galeros formations (770–750 Ma) averaged 80 + 150/-44 m/My, filling a more rapidly subsiding fault-controlled basin, consistent with the timing of regional basin formation and tectonism in Laurentian basins to the north (Fig. 10; Table 3; Halverson et al., 2020; 2022). By contrast, subsidence and sediment accumulation rates slowed substantially by ca 750 Ma, averaging 25 + 12/-5 m/My in the overlying Kwagunt Formation.

Sediment accumulation rates in the Chuar Group suggest a change in the duration of meter-scale cycles at ca. 750 Ma, and allow us to hypothesize on the origins of parasequence cyclicity. The average thickness of  $\sim$ 3.4 m for cycles in the Galeros Fm combined with the median accumulation rate of 80 m/My is consistent with pacing of cyclicity by Earth's orbital obliquity cycle, taking into account estimates for this cycle duration in the Tonian (Waltham, 2015; see also Dehler et al., 2001). The similar thickness of cycles (where expressed) in the Kwagunt Fm coupled to its slower accumulation rate suggest a transition to pacing by Earth's orbital eccentricity cycles (Meyers & Malinverno, 2018). Interestingly, this change is coincident with a postulated ca. 751 Ma glaciation that preceded the ca. 717 Ma onset of Cryogenian Snowball Earth (MacLennan et al., 2020). Obliquity and eccentricity paced cyclicity in the Chuar Group may indeed be a signal of Tonian glacioeustasy (Dehler et al., 2001). Further studies are necessary to explore the tempo and severity of global climate change between 770 and 720

The age model also helps to more precisely constrain the stratigraphic ranges of several important fossil taxa preserved in the Chuar Group and the broader ChUMP basin (Fig. 9). Of particular importance are the vase-shaped microfossils (VSMs), which are the best candidates for biostratigraphic controls in late Tonian time (Strauss et al., 2014; Riedman et al., 2018; Shields et al., 2022). The lowest confirmed report (by way of photographic documentation; Porter and Knoll, 2000: Fig. 7D) is of a VSM specimen with an agglutinated appearance (species unknown) from shales in the upper Awatubi Member on Nankoweap Butte, equivalent to an age of 741 Ma (734-747 Ma; Table 3). Horodyski (1993) reports "common" or "abundant" VSMs from several samples above this level and documents a specimen of Cycliocyrillium torquata (Porter et al. 2003) from the top of the Awatubi. Other VSM species, including Melanocyrillium hexodiadema, Bonniea dacruchares, Cycliocyrillium simplex, Trigonocyrillium fimbriatum, and T. horodyskii occur in shales from the lower Walcott Member between the Flakey Dolomite bed and the first pisolite bed (Bloeser 1985; Tingle et al., 2023), ca. 740 Ma. These VSM occurrences are strongly controlled by both sampling and preservation, but they indicate that at least by ~740 Ma, most if not all members of the Cycliocyrillium simplex faunal assemblage (Riedman et al. 2018) had appeared. This corroborates evidence from the Yukon, where VSMs (including C. simplex, C. torquata, C. rootsi, M. hexodiadema, B. dacruchares, and B. pytinaia) have been documented from the Callison Lake Formation in shales underlying strata with a Re-Os date of 752.7  $\pm$ 5.5 Ma (Table 3; Strauss et al. 2015; Cohen et al. 2017). If VSMs were as old as the lower bound of that Re-Os age (758 Ma) then our age model suggests that VSMs might be found in the Galeros Formation, perhaps as low as the Jupiter Member, if the environmental and taphonomic conditions were right.

The Chuar Group hosts other taxa that have biostratigraphic potential as well. *Cerebrosphaera globosa* (a senior synonym of *C. buickii*; see Porter and Riedman, 2016) a distinctively wrinkled vesicle interpreted to be a metabolically active cell or developing egg of a possible metazoan (Cornet et al. 2019), has been suggested as an index species for early Neoproterozoic time (i.e., late Tonian; Hill and Walter, 2000; Grey et al., 2011). Its oldest occurrence is in the Centralian Superbasin of Australia at ca. 800 Ma (Grey et al., 2011; Riedman and Sadler, 2018), and its youngest occurrence is in the Chuar Group, in the Awatubi Member at a level estimated here to be between 735 and 748 Ma in age (median = 743 Ma; see Cornet et al., 2019, for a possible occurrence in post-Sturtian, pre-Marinoan rocks, though this could reflect reworking of this relatively sturdy taxon (Cornet et al., 2019; cf. Riedman et al., 2014)). Thus, *Cerebrosphaera globosa* has an estimated stratigraphic range of ~800–743 Ma.

Lanulatisphaera laufeldii, an organic-walled vesicle characterized by filament-like spines that may coalesce to form networks, has also been

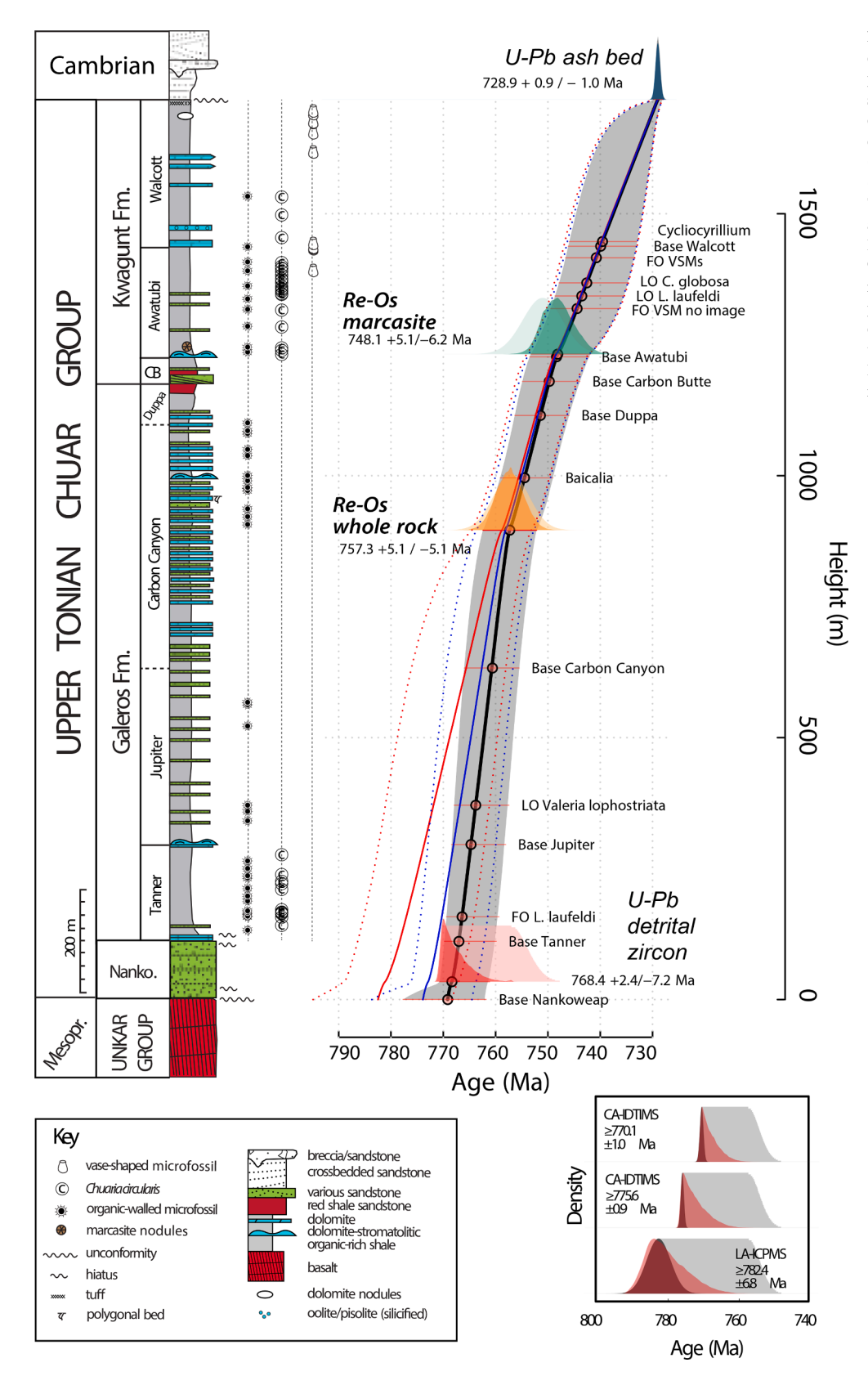


Fig. 10. Age models for the Chuar Group constructed using the modifiedBchron R package (Trayler et al., 2019). The three solid lines are the median age models considering the LA-ICP-MS-based MDA constraint for the Nankoweap Formation (red), the CA-ID-TIMS constraint at 775 Ma (blue), and the CA-ID-TIMS constraint at 770 Ma (black, favored and used for assignment of ages to stratigraphic levels). Dashed or filled envelopes represent the 95 % highest density interval of the model runs. Panels in the lower right illustrate the prior (light gray, itself constrained by the detrital zircon MDA in dark gray) and posterior (red) probability functions of the Bayesian model for the Nankoweap Formation detrital zircon sample.

proposed as a possible index fossil (Porter and Riedman, 2016). It occurs throughout the Chuar Group, including in samples that are otherwise species-poor, and has been found in at least nine other units around the world (Riedman and Sadler, 2018). Our new age model from the Chuar Group indicates that it had appeared at least by 766 Ma (759–769 Ma)

and persisted as late as 740 Ma (733-746 Ma).

Finally, Chuar Group microfossils are notable in recording among the earliest direct evidence for predation, in the form of minute (0.1 to 3.5  $\mu$ m) circular holes in a range of organic-walled microfossil species, and larger (~15–35  $\mu$ m) holes–either circular or half-moon shaped–in a

range of VSMs (Porter, 2016). The oldest of these are found in fossils at the base of the Tanner Member, constrained to be 767 Ma (760–770 Ma).

#### 6. Conclusions

New tandem U-Pb dating of Tonian detrital zircon populations in the basal Chuar Group (775.6  $\pm$  1.0 Ma; Nankoweap Formation), UMG (775.1  $\pm$  1.2 Ma; Jesse Ewing Canyon Fm), and Pahrump Group (775.4  $\pm$  1.2 Ma; Horse Thief Springs Fm) provide refined maximum depositional ages for these units and highlight the parallels in timing of "ChUMP" basin formation, paleogeography, and source area indicated by previous studies. Less common, slightly younger detrital zircons at 770.1  $\pm$  0.5 and 766.3  $\pm$  0.5 Ma in the basal Chuar and Uinta Mountain groups document even younger initiation of rifting and basin subsidence. The more accurate and precise detrital zircon maximum depositional age for the Nankoweap Formation places stronger constraints on a Bayesian age model for the Chuar Group that quantifies a basin subsidence model, and biotic and geochemical changes occurring during the Tonian leading up to the Sturtian glaciation (Dehler et al., 2001; Dehler et al., 2017).

This study demonstrates the power of a tandem geochronology workflow, harnessing the rapid throughput and low cost of LA-ICP MS to identify the youngest components of a detrital zircon spectra, and complementing it with the greater precision and accuracy of (relatively slow and expensive) CA-ID-TIMS analysis on the same crystal. In this case, the re-analysis of zircon already identified as being Neoproterozoic via LA-ICP-MS analysis significantly refined the original ages.

The igneous sources for the detrital grains in the ChUMP units remain speculative. The Gunbarrel Large Igneous Province is the closest known possible source for the 775 Ma population, as at least some of its intrusive rocks were evolved enough to contain zircon. Other possibilities include pan-Laurentian source or extra-Laurentian sources such as Tasmania/Australia, a potential conjugate block for Laurentia.

Bayesian age modelling of the Chuar Group underscores its importance as a reference section for late Tonian Earth systems predictions. Sedimentation rates appear to be faster in the earlier part of the Chuar basin evolution, which is consistent with the inception of rifting during early Chuar time. The model also constrains first and last occurrences of several short and long-lived biological events, including eukaryovorous predation (>767 Ma) and the first appearance of vase-shaped microfossils (~741 Ma, with diverse forms by 740 Ma) in the Chuar Group. The modelling can help to guide further sampling for palaeontologic and paleoclimate inquiries.

# **Declaration of Competing Interest**

The authors declare that they have no known competing financial interests or personal relationships that could have appeared to influence the work reported in this paper.

#### Data availability

Data will be made available on request.

# Acknowledgements

We thank Death Valley National Park and Grand Canyon National Park for permission to conduct research in these amazing and fragile places. Ashley National Forest of northern Utah for their field support and enthusiasm. We are grateful to the goats, llamas, dogs, colleagues, and students who made the Uinta Mountain geology part of their adventure and carried rocks. Awards to Abigail Bullard to support this project include Utah State University Department of Geosciences, the Geological Society of America, and Mount Zion United Church of Christ. Thank you to Justin Strauss, Nick Swanson-Hysell, and two anonymous

reviewers for greatly improving this manuscript. Thanks to Tony Prave, Ryan Petterson, Russell Shapiro, Jim Calzia, Stan Awramik, Dave Pierce, Ray Ingersol, and Francis Macdonald for discussions in the field. A special thank you to the Utah Geological Survey, especially Doug Sprinkel and Grant Willis, for air photo and field support in the Uintas. We acknowledge NSF grants EAR-9706541 and 1955115 for partial support.

#### Appendix A. Supplementary materials

Supplementary data to this article can be found online at https://doi.org/10.1016/j.precamres.2023.107156.

#### References

- Aleinikoff, J.N., Zartman, R.E., Walter, M., Rankin, D.W., Lyttle, P.T., Burton, W.C., 1995. U-Pb ages of metarhyolites of the Catoctin and Mount Rogers formations, central and southern Appalachians: Evidence for two pulses of Iapetan rifting. Am. J. Sci. 205, 428-454
- Allen, C.M., Campbell, I.H., 2012. Identification and elimination of a matrix-induced systematic error in LA-ICP-MS 206Pb/238U dating of zircon. Chem. Geol. 332–333, 157–165. https://doi.org/10.1016/j.chemgeo.2012.09.038.
- Bloeser, B., 1985. Melanocyrillium, a new genus of structurally complex late Proterozoic microfossils from the Kwagunt Formation (Chuar Group), Grand Canyon, Arizona. J. Paleo. 741–765.
- Box, S.E., Pritchard, C.J., Stephens, T.S., O'Sullivan, P.B., 2020. Between the supercontinents: Mesoproterozoic Deer Trail Group, an intermediate age unit between the Mesoproterozoic Belt-Purcell Supergroup and the Neoproterozoic Windermere Supergroup in northeastern Washington, USA. Can. J. Earth Sci. 57 (12), 1411–1427.
- Brennan, D.T., Li, Z.X., Rankenburg, K., Evans, N., Link, P.K., Nordsvan, A.R., Kirkland, C.L., Mahoney, J.B., Johnson, T., McDonald, B.J., 2021. Recalibrating Rodinian rifting in the northwestern United States. Geology 49 (6), 617–622.
- Bullard, A., 2018. New CA-ID-TIMS detrital zircon constriants on Middle Neoproterozoiic sedimentary successions, Southwestern United States, Department of Geoscience. Utah State University, p. 60. Masters thesis.
- Cawood, P.A., Zhao, G., Yao, J., Wang, W., Xu, Y., Wang, Y., 2018. Reconstructing South China in phanerozoic and precambrian supercontinents. Earth Sci. Rev. 186, 173–194
- Cohen, P.A., Irvine, S.W., Strauss, J.V., 2017. Vase-shaped microfossils from the Tonian Callison Lake Formation of Yukon, Canada: taxonomy, taphonomy and stratigraphic palaeobiology. Palaeontology 60 (5), 683–701.
- Condon, D.J., Schoene, B., McLean, N.M., Bowring, S.A., Parrish, R.R., 2015. Metrology and traceability of U-Pb isotope dilution geochronology (EARTHTIME Tracer Calibration Part I). Geochim. Cosmochim. Acta 164, 464–480. https://doi.org/ 10.1016/j.gca.2015.05.026.
- Cornet, Y., François, C., Compère, P., Callec, Y., Roberty, S., Plumier, J.C., Javaux, E.J., 2019. New insights on the paleobiology, biostratigraphy and paleogeography of the pre-Sturtian microfossil index taxon Cerebrosphaera. Precambr. Res. 332, 105410.
- Coutts, D.S., Matthews, W.A., Hubbard, S.M., 2019. Assessment of widely used methods to derive depositional ages from detrital zircon populations. Geosci. Front. 10, 1421–1435. https://doi.org/10.1016/j.gsf.2018.11.002.
- Dehler, C.M., Elrick, M.E., Karlstrom, K.E., Smith, G.A., Crossey, L.J., Timmons, M.J., 2001. Neoproterozoic Chuar Group (~800–742 Ma), Grand Canyon: A record of cyclic marine deposition during global cooling and supercontinent rifting. Sed. Geol. 141–142, 465–499.
- Dehler, C.M., Fanning, C.M., Link, P.K., Kingsbury, E.M., Rybczynski, D., 2010.
  Maximum depositional age and provenance of the Uinta Mountain Group and Big
  Cottonwood Formation, northern Utah: Paleogeography of rifting western Laurentia.
  Geol. Soc. Am. Bull. 122, 1686–1699.
- Dehler, C.M., Gehrels, G., Porter, S., Heizler, M., Karlstrom, K., Cox, Grant, Crossey, L.J., Timmons, J.M., 2017. Synthesis of the 780–740 Ma Chuar, Uinta Mountain, and Pahrump (ChUMP) groups, western USA: Implications for Laurentia-wide cratonic marine basins. GSA Bulletin 129 (5–6). 607–624. https://doi.org/10.1130/2016361.
- Ding, H., Kohn, M.J., Zhang, Z., 2021. Long-lived (ca. 22–24 Myr) partial melts in the eastern Himalaya: Petrochronologic constraints and tectonic implications. Earth Planet. Sci. Lett. 558, 116764.
- Ford, T.D., Breed, W.J., 1973. Late Precambrian Chuar Group, Grand Canyon. Arizona. Geol. Soc. Am. Bull. 84, 1243–1260.
- Grey, K., Hill, A.C., Calver, C., 2011. Chapter 8 Biostratigraphy and stratigraphic subdivision of Cryogenian successions of Australia in a global context. Geol. Soc. London Memoirs 36 (1), 113–134.
- Grimes, C.B., Wooden, J.L., Cheadle, M.J., John, B.E., 2015. "Fingerprinting" tectonomagmatic provenance using trace elements in igneous zircon. Contrib. Miner. Petrol. 170, 1–26. https://doi.org/10.1007/s00410-015-1199-3.
- Harlan, S.S., 1993. New paleomagnetic results from Middle and Late Proterozoic intrusive rocks of the central and southern Rocky Mountains. Geol. Soc. Am. Abstr. Programs 25, 48.
- Harlan, S.S., Geissman, J.W., Snee, L.W., 1997. Paleomagnetic and 40Ar/39Ar geochronologic data from Late Proterozoic mafic dikes and sills, Montana and Wyoming. US Government Printing Office, p. (p. 1580)..

- Haslett, J., Parnell, A., 2008. A simple monotone process with application to radiocarbon-dated depth chronologies. J. Roy. Stat. Soc.: Ser. C (Appl. Stat.) 57 (4), 399,418
- Herriott, T.M., Crowley, J.L., Schmitz, M.D., Wartes, M.A., Gillis, R.J., 2019. Exploring the law of detrital zircon: LA-ICP-MS and CA-TIMS geochronology of Jurassic forearc strata, Cook Inlet, Alaska, USA. Geology 47, 1044–1048. https://doi.org/10.1130/ G46312.1.
- Hill, A.C., Walter, M.R., 2000. Mid-Neoproterozoic (~830–750 Ma) isotope stratigraphy of Australia and global correlation. Precambr. Res. 100 (1–3), 181–211.
- Horodyski, R.J., 1993. Paleontology of Proterozoic shales and mudstones: Examples from the Belt Supergroup, Chuar Group, and Pahrump Group v. 61, 241–278.
- Jaffey, A.H., Flynn, K.F., Glendenin, L.E., Bentley, W.C., Essling, A.M., 1971. Precision measurements of half-lives and specific activities of <sup>235</sup>U and <sup>238</sup>U. Phys. Rev. C 4, 1889–1906.
- Jefferson, C.W., Parrish, R.R., 1989. Late Proterozoic stratigraphy, U-Pb zircon ages, and rift tectonics, Mackenzie Mountains, northwestern Canada. Can. J. Earth Sci. 26 (9), 1784–1801.
- Jing, X., Evans, D.A., Yang, Z., Tong, Y., Xu, Y., Wang, H., 2021. Inverted South China: A novel configuration for Rodinia and its breakup. Geology 49 (4), 463–467.
- Karlstrom, K.E., Bowring, S.A., Dehler, C.M., Knoll, A.H., Porter, S.M., Marais, D.J.D., Weil, A.B., Sharp, Z.D., Geissman, J.W., Elrick, M.B., Timmons, J.M., 2000. Chuar Group of the Grand Canyon: Record of breakup of Rodinia, associated change in the global carbon cycle, and ecosystem expansion by 740 Ma. Geology 28 (7), 619–622.
- Li, Z.X., Bogdanova, S., Collins, A.S., Davidson, A., De Waele, B., Ernst, R.E., Fitzsimons, I.C.W., Fuck, R.A., Gladkochub, D.P., Jacobs, J., Karlstrom, K.E., 2008. Assembly, configuration, and break-up history of Rodinia: a synthesis. Precamb. Res. 160 (1–2), 179–210.
- Li, Z.X., Evans, D.A., Halverson, G.P., 2013. Neoproterozoic glaciations in a revised global palaeogeography from the breakup of Rodinia to the assembly of Gondwanaland. Sediment. Geol. 294, 219–232.
- Licari, G.R., 1978. Biogeology of the late pre-Phanerozoic Beck Spring Dolomite of eastern California. J. Paleo. 767–792.
- Macdonald, F.A., Yonkee, W.A., Flowers, R.M. and Swanson-Hysell, N.L., 2023. Neoproterozoic of Laurentia.
- Macdonald, F.A., Schmitz, M.D., Strauss, J.V., Halverson, G.P., Gibson, T.M., Eyster, A., Cox, G., Mamrol, P., Crowley, J.L., 2018. Cryogenian of Yukon. Precambr. Res. 319, 114–143. https://doi.org/10.1016/j.precamres.2017.08.015.
- Mackinder, A., Cousens, B.L., Ernst, R.E., Chamberlain, K.R., 2019. Geochemical, Isotopic, and U-Pb zircon study of the central and southern portions of the 780 Ma Gunbarrel Large Igneous Province in western Laurentia. Canadian J. Earth Sci. 56, 738–755. https://doi.org/10.1139/cjes-201-0083.
- MacLennan, S.A., Eddy, M.P., Merschat, A.J., Mehra, A.K., Crockford, P.W., Maloof, A.G., Southworth, C.S., Schoene, B., 2020. Geologic evidence for an icehouse Earth before the Sturtian global glaciation. *Science*. Advances 6 (24), p.eaay6647.
- Mahon, R.C., Dehler, C.M., Link, P.K., Karlstrom, K.E., Gehrels, G.E., 2014a.
  Supplemental material: Geochronologic and stratigraphic constraints on the Mesoproterozoic and Neoproterozoic Pahrump Group, Death Valley, California: A record of the assembly, stability, and breakup of Rodinia. Geological Society of America. Journal contribution. https://doi.org/10.1130/2014108.
- America. Journal contribution. https://doi.org/10.1130/2014108.

  Mahon, R.C., Dehler, C.M., Link, P.K., Karlstrom, K.E., Gehrels, G.E., 2014b.
  Geochronologic and stratigraphic constraints on the Mesoproterozoic and
  Neoproterozoic Pahrump Group, Death Valley, California: a record of the assembly
  and breakup of Rodinia. Geol. Soc. Am. Bull. 126 (5–6), 619–638.
- Mattinson, J.M., 2005. Zircon U-Pb chemical abrasion ("CA-TIMS") method: combined annealing and multi-step partial dissolution analysis for improved precision and accuracy of zircon ages. Chem. Geol. 220 (1), 47–66.
- Maud, R.L., 1979. Stratigraphy and depositional environments of the carbonateterrigenous member of the Crystal Spring Formation, Death Valley, California, (M. S. Thesis), Penna, State Univ., 177.
- McLean, N.M., Condon, D.J., Schoene, B., Bowring, S.A., 2015. Evaluating uncertainties in the calibration of isotopic reference materials and multi-element isotopic tracers (EARTHTIME Tracer Calibration Part II). Geochim. Cosmochim. Acta 164, 481–501. https://doi.org/10.1016/j.gca.2015.02.040.
- Meyers, S.R., Malinverno, A., 2018. Proterozoic Milankovitch cycles and the history of the solar system. Proc. Nat. Acad. Sci. 115, 6363–6368. https://doi.org/10.1073/ pnas.1717689115.
- Milton, J.E., Hickey, K.A., Gleeson, S.A., Friedman, R.M., 2017. New U-Pb constraints on the age of the Little Dal Basalts and Gunbarrel-related volcanism in Rodinia. Precambrian Research, v 296, 168–180. https://doi.org/10.1016/j. precamres.2017.04030.
- Morais, L., Lahr, D.J.G., Rudnitzki, I.D., Freitas, B.T., Romero, G.R., Porter, S.M., Knoll, A.H., Fairchild, T.R., 2019. Insights into vase-shaped microfossil diversity and Neoproterozoic biostratigraphy in light of recent Brazilian discoveries. J. Paleo. 93 (4), 612–627.
- Mulder, J.A., Everard, J.L., Cumming, G., Meffre, S., Bottrill, R.S., Merdith, A.S., Halpin, J.A., McNeill, A.W., Cawood, P.A., 2020. Neoproterozoic opening of the Pacific Ocean recorded by multi-stage rifting in Tasmaniam, Australia. Earth-Sci. Phys. 201, 103041.
- Nasdala, L., Lengauer, C.L., Hanchar, J.M., Kronz, A., Wirth, R., Blanc, P., Kennedy, A.K., Seydoux-Guillaume, A.M., 2002. Annealing radiation damage and the recovery of cathodoluminescence. Chem. Geol. 191, 121–140.
- Park, Y., Swanson-Hysell, N.L., Xian, H., Zhang, S., Condon, D.J., Fu, H., Macdonald, F. A., 2021. A consistently high-latitude South China from 820 to 780 Ma: implications for Exclusion from Rodinia and the feasibility of large-scale true polar wander. J. Geophys. Res.: Solid Earth 126 (6) e2020JB021541.

- Porter, S.M., 2016. 2016, Tiny vampires in ancient seas: evidence for predation via perforation in fossils from the 780–740 million-year-old Chuar Group, Grand Canyon, USA. Proc. R. Soc. B. 283, 20160221.
- Porter, S.M., Knoll, A.H., 2000. Testate amoebae in the Neoproterozoic Era: evidence from vase-shaped microfossils in the Chuar Group, Grand Canyon. Paleobiology 26, 360–385.
- Porter, S.M., Meisterfeld, R., Knoll, A.H., 2003. Vase-shaped microfossils from the Neoproterozoic Chuar Group, Grand Canyon: a classification guided by modern testate amoebae. J. Paleo. 77 (3), 409–429.
- Porter, S.M., Riedman, L.A., 2016. Systematics of organic-walled microfossils from the ca. 780–740 Ma Chuar Group, Grand Canyon, Arizona. J. Paleo. 90 (5), 815–853.
- Riedman, L.A., Sadler, P.M., 2018. Global species richness record and biostratigraphic potential of early to middle Neoproterozoic eukaryote fossils. Precambr. Res. 319, 6–18.
- Riedman, L.A., Porter, S.M., Halverson, G.P., Hurtgen, M.T., Junium, C.K., 2014.
  Organic-walled microfossil assemblages from glacial and interglacial Neoproterozoic units of Australia and Svalbard. Geology 42 (11), 1011–1014.
- Riedman, L.A., Porter, S.M., Calver, C.R., 2018. Vase-shaped microfossil biostratigraphy with new data from Tasmania, Svalbard, Greenland, Sweden and the Yukon. Precambr. Res. 319, 19–36.
- Riedman, L.A., Porter, S.M., Czaja, A.D., 2021. Phosphatic scales in vase-shaped microfossil assemblages from Death Valley, Grand Canyon, Tasmania, and Svalbard. Geobiology 19 (4), 364–375.
- Rooney, A.D., Austermann, J., Smith, E.F., Li, Y., Selby, D., Dehler, C.M., Schmitz, M.D., Karlstrom, K.E., Macdonald, F.A., 2018. Coupled Re-Os and U-Pb geochronology of the Tonian Chuar Group, Grand Canyon. Geol. Soc. Am. Bull.
- Rybczynski, D., 2009, Correlation, paleogeography, and provenance of the eastern Uinta Mountain Group, Goslin Mountain area, Daggett County, northeastern Utah [M.S. thesis]: Logan, Utah State University, 224 p.
- Schmitz, M.D., Schoene, B., 2007. Derivation of isotope ratios, errors, and error correlations for U-Pb geochronology using 205Pb-235U-(233U)-spiked isotope dilution thermal ionization mass spectrometric data. Geochem. Geophys. Geosyst. 8 (8).
- Shields, G.A., Strachan, R.A., Porter, S.M., Halverson, G.P., Macdonald, F.A., Plumb, K.
   A., De Alvarenga, C.J., Banerjee, D.M., Bekker, A., Bleeker, W., Brasier, A., 2022.
   A template for an improved rock-based subdivision of the pre-Cryogenian timescale.
   J. Geol. Soc. London 179 (1).
- Sláma, J., Košler, J., Condon, D.J., Crowley, J.L., Gerdes, A., Hanchar, J.M., Horstwood, M.S.A., Morris, G.A., Nasdala, L., Norberg, N., Schaltegger, U., Schoene, B., Tubrett, M.N., Whitehouse, M.J., 2008. Plešovice zircon — A new natural reference material for U-Pb and Hf isotopic microanalysis. Chem. Geol. 249, 1–35.
- Smith, E.F., MacDonald, F.A., Crowley, J.L., Hodgin, E.B., Schrag, D.P., 2016.
   Tectonostratigraphic evolution of the c. 780–730 Ma Beck Spring Dolomite: Basin Formation in the core of Rodinia. Geol. Soc. Lond. Spec. Publ. 424 (1), 213–239.
- Strauss, J.V., Rooney, A.D., Macdonald, F.A., Brandon, A.D., Knoll, A.H., 2014. 740 Ma vase-shaped microfossils from Yukon, Canada: Implications for Neoproterozoic chronology and biostratigraphy. Geology 42 (8), 659–662.
- Strauss, J.V., MacDonald, F.A., Halverson, G.P., Tosca, N.J., Schrag, D.P., Knoll, A.H., 2015. Stratigraphic evolution of the Neoproterozoic Callison Lake Formation: Linking the break-up of Rodinia to the Islay carbon isotope excursion. Am. J. Sci. 315 (10), 881–944.
- Timmons, M.J., Karlstrom, K.E., Dehler, C.M., Geissman, J.W., Heizler, M.T., 2001. Proterozoic multistage (~1.1 and ~0.8 Ga) extension in the Grand Canyon Supergroup and establishment of northwest and north-south tectonic grains in the southwestern United States. Geol. Soc. Am. Bull. 113, 163–181.
- Tingle, K.E., Porter, S.M., Raven, M.R., Czaja, A.D., Webb, S.M., 2023. Organic preservation of vase-shaped microfossils from the late Tonian Chuar Group, Grand Canyon, Arizona, USA. Geobiology. https://doi.org/10.1111/gbi.12544.
- Trayler, R., Schmitz, M., Cuitiño, J., Kohn, M., Bargo, M.S., Kay, R., Stromberg, C., Vizcaíno, S., 2019. An improved approach to age-modeling in deep time: Implications for the Santa Cruz Formation. Argentina. GSA Bulletin. 132 https://doi.org/10.1130/B35203.1.
- Turner, N.J., Black, L.P., Kamperman, M., 1998. Dating of Neoproterozoic and Cambrian orogenies in Tasmania. Aust. J. Earth Sci. 45 (5), 789–806.
- Vermeesch, P., 2021. Maximum depositional age estimation revisited. Geosci. Front. v. 12, 843–850. https://doi.org/10.1016/j.gsf.2020.08.008.
- Waltham, D., 2015. Milankovitch period uncertainties and their impact on cyclostratigraphy. J. Sediment. Res. 85, 990–998. https://doi.org/10.2110/ ier.2015.66
- Xian, H., Zhang, S., Li, H., Yang, T., Wu, H., 2020. Geochronological and palaeomagnetic investigation of the Madiyi Formation, lower Banxi Group, south China: Implications for Rodinia reconstruction. Precambr. Res. 336, 105494.

#### Further reading

- Butterfield, N.J., 2007. Macroevolution and macroecology through deep time. Palaeontology 50 (1), 41–55.
- Davydov, V.I., Crowley, J.L., Schmitz, M.D., Poletaev, V.I., 2010. High-precision U–Pb zircon age calibration of the global Carboniferous time scale and Milankovitch band cyclicity in the Donets Basin, eastern Ukraine. Geochemistry, Geophysics, Geosystems 1, Q0AA04.
- Frimmel, H.E., Klötzli, U.S., Siegfried, P.R., 1996. New Pb-Pb single zircon age constraints on the timing of Neoproterozoic glaciation and continental break-up in Namibia. J. Geol. 104 (4), 459–469.

- Frimmel, H.E., Basei, M.S., Gaucher, C., 2011. Neoproterozoic geodynamic evolution of SW-Gondwana: A southern African perspective. Int. J. Earth Sci. 100, 323–354.
- Halverson, G.P., Kunzmann, M., Strauss, J.V., Maloof, A.C., 2018. The Tonian-Cryogenian transition in Northeastern Svalbard. Precambr. Res. 319, 79–95.
- Halverson, G.P., Shen, C., Davies, J.H., Wu, L., 2022. A Bayesian approach to inferring depositional ages applied to a late Tonian reference section in Svalbard. Front. Earth Sci. 10, 106.
- Harlan, S.S., Heaman, L., LeCheminant, A.N., Premo, W.R., 2003. Gunbarrel mafic magmatic event: A key 780 Ma time marker for Rodinia plate reconstructions. Geology 31 (12), 1053–1056.
- Li, Z.X., Li, X.H., Kinny, P.D., Wang, J., Zhang, S., Zhou, H., 2003. Geochronology of Neoproterozoic syn-rift magmatism in the Yangtze Craton, South China and correlations with other continents: evidence for a mantle superplume that broke up Rodinia. Precambr. Res. 122 (1–4), 85–109.
- Macdonald, F.A., Schmitz, M.D., Crowley, J.L., Roots, C.F., Jones, D.S., Maloof, A.G., Strauss, J.V., Cohen, P.A., Johnston, D.T., Schrag, D.P., 2010. Calibrating the cryogenian. Science 327 (5970), 1241–1243.
- Merschat, A.J., Southworth, S., McClellan, E., Tollo, R.P., Rankin, D.W., Hooper, S., Bauer, S., 2014. Key structural and stratigraphic relationships from the northeast end of the Mountain City window and the Mount Rogers area. Virginia-North. Carolina—Tennessee.

- Mulder, J.A., Karlstrom, K.E., Halpin, J.A., Merdith, A.S., Spencer, C.J., Berry, R.F., McDonald, B., 2019. Rodinian devil in disguise: Correlation of 1.25–1.10 Ga strata between Tasmania and Grand Canyon. Geology 46, 991–994. https://doi.org/ 10.1130/G45225.1.
- Porter, S.M., Agić, H., Riedman, L.A., 2018. Anoxic ecosystems and early eukaryotes. Emerg. Top. Life Sci. 2 (2), 299–309.
- Poulsen, C.J., Tabor, C., White, J.D., 2015. Long-term climate forcing by atmospheric oxygen concentrations. Science 348 (6240), 1238–1241.
- Rankin, Douglas W. 1993. The volcanogenic Mount Rogers Formation and the overlying 59 glaciogenic Konnarock Formation: Two late Proterozoic units in southwestern Virginia. Washington, D.C., Denver, CO: U.S. G.P.O., U.S. Geological Survey, Map Distribution.
- Riedman, L.A., Porter, S., 2016. Organic-walled microfossils of the mid-Neoproterozoic Alinya Formation, Officer Basin, Australia. J. Paleontol. 90 (5), 854–887.
- Wang, C., Lechte, M.A., Reinhard, C.T., Asael, D., Cole, D.B., Halverson, G.P., Porter, S. M., Galili, N., Halevy, I., Rainbird, R.H., Lyons, T.W., 2022. Strong evidence for a weakly oxygenated ocean–atmosphere system during the Proterozoic. Proc. Nat. Acad. Sci. 119 (6), e2116101119.
- Xu, B., Xiao, S., Zou, H., Chen, Y., Li, Z.X., Song, B., Liu, D., Zhou, C., Yuan, X., 2009. SHRIMP zircon U-Pb age constraints on Neoproterozoic Quruqtagh diamictites in NW China. Precambr. Res. 168 (3–4), 247–258.